KTH ROYAL INSTITUTE
OF TECHNOLOGY

Doctoral Thesis in Physics

MELCOR Capability Development for Simulation of Debris Bed Coolability

YANGLI CHEN

Stockholm, Sweden 2021

MELCOR Capability Development for Simulation of Debris Bed Coolability

YANGLI CHEN

Academic Dissertation which, with due permission of the KTH Royal Institute of Technology, is submitted for public defence for the Degree of Doctor of Philosophy on Thursday, September 23, 2021, at 9:30 a.m. in AlbaNova University Center, Stockholm.

Doctoral Thesis in Physics
KTH Royal Institute of Technology
Stockholm, Sweden 2021

TRITA-SCI-FOU 2021:31
ISBN: 978-91-7873-972-1

Printed by: Universitetsservice US-AB, Sweden 2021

Abstract

The severe accident management (SAM) strategy for a Nordic boiling water reactor (BWR) employs cavity flooding prior to vessel failure, so that the core melt (corium) discharged from the vessel could fragment and form a particulate debris bed. The key to the success of this SAM strategy is the coolability of ex-vessel debris beds.

The safety analysis involves knowledge about the reactor response to severe accidents under this SAM strategy, which requires the integral simulation of a system code such as MELCOR. Since currently the MELCOR code lacks the modeling of ex-vessel particulate debris beds, the present study aims to develop the capability of MELCOR for the simulation of debris bed coolability through the coupling of MELCOR with other codes, which are dedicated to this phenomenon.

The study is started from the qualification of a MELCOR model for severe accident analysis of a reference Nordic BWR, with the aim to help identify a proper core nodalization. For this purpose, three different core meshes (coarse, medium, and fine) are employed to obtain their impacts on corium release conditions. It is found the coarse mesh is sufficient in the present study, since it is not only computationally efficient, but also predicting earlier vessel failure and faster corium release, providing a more conservative condition for debris bed coolability analysis.

Two couplings are then adopted: (i) coupling of MELCOR with the COCOMO code, which is a mechanistic code for simulation of thermal hydraulics in debris beds; and (ii) coupling of MELCOR with a surrogate model developed in the present study. The first method can simulate the transient behavior of a debris bed during quench process. The second method can efficiently predict the coolability limit (dryout power) required in safety analysis. The surrogate model is developed based on the COCOMO prediction of two-dimensional debris beds.

The developed simulation tools, including the coupled codes and the surrogate model, are applied to the safety analysis of the reference Nordic BWR. The coupled MELCOR/COCOMO simulation is used to investigate the debris bed properties. The effective particle diameter is found as approximately 10% larger than the surface mean diameter of a debris bed with distributed sizes, quantified by the quench rate. For the effect of

debris bed shape, it shows a faster quench process with a lower bed slope angle. The quench front propagation as well as the responses of local temperature and containment pressure are obtained.

The coupled MELCOR/surrogate model simulation is performed to estimate the coolability of ex-vessel vessel debris beds. The results show that debris beds are coolable under prototypical conditions with probable bed properties. The surrogate model is used to generate coolability maps, which show the debris bed coolability with the variation of bed properties. The sensitivity analysis indicates that the porosity and the geometry are the most influential to coolability limit. An uncertainty analysis methodology is proposed to obtain the probability of non-coolable debris beds.

Keywords: Severe accident, coolability, MELCOR, COCOMO, surrogate modeling, coupling codes, uncertainty analysis.

Sammanfattning

Strategin för hantering av svåra haverier (SAM) från ett vattenfyllt nedre primärutrymme för nordiska kokvattenreaktorerna (BWR), så att härdsmältan (corium) som läckt ut från reaktortanken kan fragmentera och bilda en partikelformiggrusbädd. Nyckeln till framgången med denna SAM-strategi är kylbarheten av härdsmältan efter genomsmältning av reaktortanken (ex-vessel).

Säkerhetsanalysen fordrar kunskap om reaktorns respons på svåra haverier enligt denna SAM-strategi, detta kräver en integrerad simulering av händelsen med en systemkod, som MELCOR. Eftersom MELCOR för närvarande saknar modellering av grusbäddar efter genomsmältning av reaktortanken, syftar denna studie på att utveckla MELCOR:s förmåga att simulera grusbäddars kylbarhet genom koppling av MELCOR till andra koder som är avsedda för detta fenomen.

Studien utgår från utvärdering av en MELCOR-modell för analys av svåra haverier i en representativmodell för en nordisk kokarvattenreaktor. Syftet är att identifiera en korrekt härd nodalisering. Tre olika nodtyper (grovmaskig, medelmaskig och finmaskig) för nodalisering av härden används för att studera deras effekt på simuleringen av härdsmältans utsläpp. Den grovmaskiga nodaliseringen bedömdes lämpligast för den nuvarande studien, eftersom det inte bara är beräkningseffektivt, utan även förutspår tidigare reaktortankbrått och snabbare utsläpp av härdsmältan, vilket ger ett mer konservativt tillstånd för analys av kylbarhet av grusbädden.

Två kopplingar antas sedan: i) koppling av MELCOR med den mekaniska koden COCOMO avsedd för simulering av termohydraulik i grusbäddar; och ii) koppling av MELCOR med en surrogatmodell utvecklad under denna studie. Den första metoden kan simulera störningar hos en grusbädd under kylningsprocessen. Den andra metoden kan effektivt förutsäga marginalerna mot torrkokning (dryout power) som krävs i säkerhetsanalysen. Surrogatmodellen är utvecklad baserat på COCOMOs-förutsägelsen av tvådimensionella grusbäddar.

De utvecklade simuleringsverktygen, inklusive de koppladekoderna och surrogatmodellen, tillämpas på säkerhetsanalysen av en referens nordisk kokarvattenreaktor BWR. Den kopplade MELCOR/COCOMO simuleringen används för att undersöka grusbäddens egenskaper. Den effektiva partikeldiametern är cirka 10% större än medeldiameter i för grusbäddsytaspartiklar med distribuerade partikelstorlekar som kvantifierats av snabbt nedkylningshastigheten. Grusbäddens form påverkar effekten av nedkylningsprocessen, en lägre lutningsvinkel ökar nedkylningen. Nedkylningsfrontens utbredning så som den lokala temperatur och inneslutningstrycket erhålls.

Den kopplade MELCOR/surrogatmodellsimuleringen utförs för att uppskatta kylbarheten hos grusbäddar efter genomsmältning av reaktortanken. Resultaten visar att grusbäddar kan kylas under prototypiska förhållanden med sannolika grusbäddegenskaper. Surrogatmodellen används för att generera kylbarhetskartor, som beskriver systematiskt grusbäddens kylbarhet beroende på variation i grusbäddegenskaper. Känslighetsanalyser indikerar att porositet och geometrin är mest inflytelserika för marginalerna mot torrkokning. En metod för osäkerhetsanalys föreslås för att för att erhålla sannolikheten för en icke kylbargrusbädd.

Nyckelord: Svåra haveri, kylbarhet, MELCOR, COCOMO, surrogatmodellering, koppladekoder, osäkerhetsanalys.

List of appended papers

Publications included in this thesis

Paper 1 **Chen, Y.**, Zhang, H., Villanueva, W., Ma, W. and Bechta, S., 2019. A sensitivity study of MELCOR nodalization for simulation of in-vessel severe accident progression in a boiling water reactor. Nuclear Engineering and Design, 343, pp.22-37. DOI: 10.1016/j.nucengdes.2018.12.011.

Paper 2 **Chen, Y.**, Zhang, H., and Ma, W., 2022. Coupled MELCOR /COCOMO Analysis on Quench of Ex-Vessel Debris Beds. Annals of Nuclear Energy, 165, 108643. DOI: 10.1016/j.anucene.2021.108643.

Paper 3 **Chen, Y.** and Ma, W., 2020. Development and application of a surrogate model for quick estimation of ex-vessel debris bed coolability. Nuclear Engineering and Design, 370, p.110898. DOI: 10.1016/j.nucengdes.2020.110898.

Author's contribution to the included publications

Yangli Chen made major contributions to the publications of all the above articles under the guidance of supervisors and with the collaboration of other co-authors, including conceptualization, methodology, code implementation, calculation and analysis, and writing the draft.

Publications not included in this thesis

I **Chen, Y.**, Ma W., 2020. Uncertainty quantification for TRACE simulation of FIX-II No. 5052 test. Annals of Nuclear Energy, 143, 107490. DOI: 10.1016/j.anucene.2020.107490.

II **Chen, Y.**, Ma W., 2017. Sensitivity and Uncertainty Analysis of TRACE Simulation Against FIX-II Experiments. Proceedings of 17th Topical Meeting on Nuclear Reactor Thermal Hydraulics (NURETH-17), Xi'an, China.

III **Chen, Y.**, Zhang, H., Villanueva, W., Ma, W. and Bechta, S., 2018. A Nodal Sensitivity Study of MELCOR Simulation of

In-Vessel Severe Accident Progression in a Nordic BWR. Proceedings of 12th International Topical Meeting on Nuclear Reactor Thermal-Hydraulics, Operation and Safety (NUTHOS-12), Qingdao, China.

IV **Chen, Y.**, Ma W., 2019. Development of Surrogate Model for Debris Bed Coolability Analysis. Proceedings of 18th Topical Meeting on Nuclear Reactor Thermal Hydraulics (NURETH-18), Portland, U.S.A.

V Wang, H., Villanueva, W., **Chen, Y.**, Kulachenko, A. and Bechta, S., 2021. Thermo-mechanical behavior of an ablated reactor pressure vessel wall in a Nordic BWR under in-vessel core melt retention. Nuclear Engineering and Design, 379, p.111196. DOI:10.1016/j.nucengdes.2021.111196.

VI Zhao, N., **Chen, Y.**, Ma, W., Bechta, S. and Isaksson, P., 2021. A nodal sensitivity study of MELCOR simulation for severe accidents in a pressurized water reactor. Annals of Nuclear Energy, 160, p.108373. DOI: 10.1016/j.anucene.2021.108373.

Acknowledgements

I would first like to express my sincere gratitude to my supervisor, Prof. Weimin Ma, for providing me the valuable opportunity of doctoral study, the professional guidance from his expert vision, the inspiring discussions, and the positive influence by his personality and patience.

I would like to thank my co-supervisor, Prof. Sevostian Bechta, who always offers me enlightening thoughts and insightful comments. I am very thankful to Dr. Walter Villanueva for valuable discussions. I would like to thank to Dr. Michael Buck for the valuable guidance on the COCOMO code, and to Mr. Huimin Zhang for generously sharing me his research resources. I am also very grateful to Prof. Henryk Anglart for reviewing the draft of the thesis, and to Mr. Sean Roshan Ghias for the help with the abstract translation.

I am grateful to all colleagues at Division of Nuclear Power Safety for providing me the warm and friendly environment.

I wish to thank all my friends. Thank you Liyun, Hongdi and Ruicun, who accompany me every time I need during these years.

Thanks to the little cat Rosie's company.

Last and most importantly, I want to express my deepest gratitude to my mom Ms. Shujun Yang, my dad Mr. Jianxiu Chen, and my boyfriend Dr. Wenyuan Fan for giving me love and support.

Financial supports from Consortium of SSM and NPPs in Sweden (APRI), Swedish Radiation Safety Authority (SSM), and Swiss Federal Nuclear Safety Inspectorate (ENSI) are acknowledged. The support from the China Scholarship Council (CSC) is specially acknowledged for making my doctoral study possible. Special thanks to IKE of University of Stuttgart for providing the COCOMO code.

Table of Contents

List of figures

List of tables

Nomenclature

c_p	isobaric specific heat [J/(kg·K)]
d	particle diameter (m)
D	dimension
e	specific internal energy (J/kg)
f	characteristic factor
g	gravitational acceleration constant (m/s²)
h	heat transfer coefficient [W/(m²·K)]
h_{fg}	latent heat of vaporization (J/kg)
i	specific enthalpy (J/kg)
Ja	Jakob number
k	conductivity [W/(m·K)]
K	friction coefficient
N	sample size
Nu	Nusselt number
p	pressure (Pa)
Pr	Prandtl number
Q	heat flux (W/m²)
q'	dryout power density (W/kg)
Re	Reynolds number
s	saturation
S	Sobol index
S_T	Sobol index of total effect
t	time (s)

T	temperature (K)
v	velocity (m/s)
V	variance
W	weight function
X	input parameter
Y	output parameter

Greek letters

η	passability
ε	porosity
κ	permeability
μ	dynamic viscosity [kg/(m·s)]
ρ	density (kg/m^3)
ρ_s	Spearman correlation coefficient
σ	surface tension (N/m)
Γ	mass transfer rate [kg/(m^3·s)]

Subscripts

FM	full model
g	gas
i, j, k	iterator
l	liquid
max	maximum
min	minimum
r	relative
s	solid
sat	saturation
SM	surrogate model

Superscripts

B	bubbly flow
D	droplet flow
eff	effective
evap	evaporation
FB	film boiling
PB	pool boiling
trans	transition

List of acronyms

ADS	automatic depressurization system
BWR	boiling water reactor
CAV	cavity
CCFL	counter-current flow limitation
CDF	cumulative distribution fuction
DHF	dryout heat flux
DINAMO	direct interface for adding models
ECCS	emergency core cooling system
FCI	fuel-coolant interaction
LOCA	loss-of-coolant accident
LWR	light water reactor
MTD	modified Tung-Dhir model
NPP	nuclear power plant
PDF	probabilistic density function
PSA	probabilistic safety analysis
SAM	severe accident management
SBO	station blackout
SMT	surrogate modeling toolbox
SNAP	symbolic nuclear analysis package

1 Introduction

1.1 Severe accident management strategy

The Fukushima accident gathered the world's concern on the severe accident of nuclear power plants (NPPs). For Nordic-type boiling water reactors (BWRs), the severe accident management (SAM) strategy is to flood the lower drywell with water stored in the lower wetwell, so the core melt (corium) is expected to fall and stabilize in the deep water pool underneath the vessel, as the schematic shown in Figure 1.1 [1].

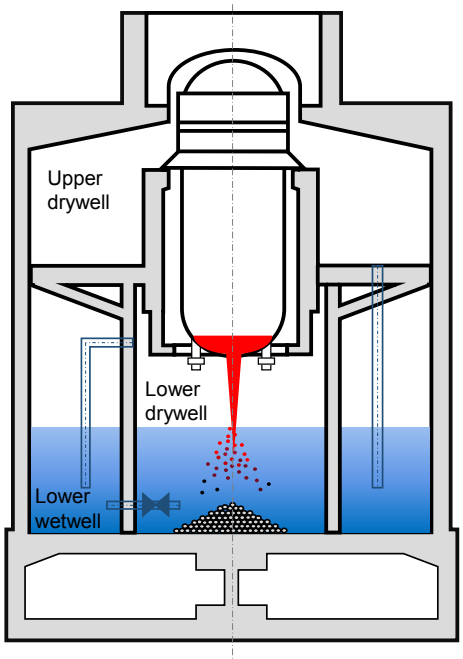

Figure 1.1 Schematic of SAM strategy features in Nordic BWRs.

Under a hypothetical severe accident condition, the potential failure of the lower head penetrations provides pathways for the discharge of molten corium in the vessel [2]. The molten corium falls in the deep water pool and fragments into millimeter-scale droplets which solidify and settle down on the cavity floor, forming a particulate debris bed according to some experimental observations [3], [4]. The fuel-coolant interactions (FCI) between the molten corium and the water are extremely complicated in hydrodynamic and thermal aspects, and even possibly explosive [5]. There are two key questions which need to be addressed for this SAM strategy: (i) avoiding any possible steam explosion that is energetic enough to threaten the containment integrity, and (ii) stabilizing the so-formed debris bed in the deep water pool.

1.2 Debris bed coolability

Since coolability of a debris bed, i.e., the effective removal of the decay heat in the debris bed by natural convection of two-phase flow of water and steam, is the major condition for reaching ex-vessel stabilization, it should be analyzed in the qualification of the SAM strategy. The debris bed coolability analysis can be conducted in two stages during the accident progression: (1) quenching of hot debris particles initially settled on the cavity floor, and (2) long-term cooling of the quenched particles.

Quenching of the debris bed is a transient process, starting from the initially dry debris bed with high-temperature particles formed from FCI, until debris bed fully cooled down by water. Before the quench front reaches, the temperature of the dry particles would continuously increase due to the decay power. It is essential to know how the quench front propagates in the debris bed, and whether the bed can be quenched before the local particles reach oxidation or melting temperature. The successful quench of the debris bed is the prerequisite to achieve the stabilization in a long term. Though the large temperature difference between particles and water bring difficulties for measurement, several experiments on the quench of hot particle beds with either top or bottom flooding have provided valuable observations [6]–[10].

After debris bed is quenched, the steady-state cooling, that the decay heat is removed by two-phase flow without reaching an elevated temperature of debris particles, is expected for a long term. The long-term coolability of the debris bed is limited by the dryout heat flux (DHF), which is the maximum heat flux for decay heat removal prior to the occurrence of

dryout in the debris bed. If the decay heat flux exceeds the DHF, it is the starting point for the temperature of the debris bed to escalate locally or extensively, even leading to re-melting of the debris bed if the decay heat is high enough. Therefore, the long-term coolability is conservatively considered as achieved if the decay heat flux of the debris bed is less than the DHF [11]. Experimental investigations have been conducted to measure the DHF, using the packed particle bed to mimic the prototypical debris bed, with electrical or induction heating [12]–[16]. To perform experimental measurements, the heating power of the particles is gradually increased until the local measurement of the temperature increases sharply above the saturation temperature of the pool, indicating the occurrence of dryout.

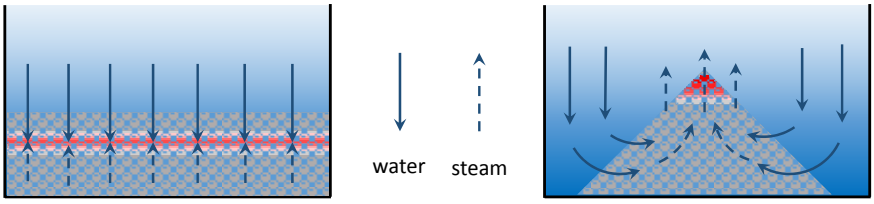

(a) one-dimensional (b) multi-dimensional

Figure 1.2 Schematics of two phase flow within debris bed.

Driven by different flow patterns as shown in Figure 1.2, the debris bed cooling mechanism is relevant to the bed geometry. The definitions of one-dimensional (1D) and multi-dimensional debris bed are based on the dimension of coolant velocity. The 1D debris bed is assumed as an ideal scenario when the debris bed fully covers the cavity floor with a constant thickness. The coolability limit is governed by the countercurrent flow limitation (CCFL), when the steam flow prevents the water penetration. Analytical or empirical correlations were proposed for 1D debris bed to calculate the global parameters of quench process, e.g., steam flow rate or the quench front velocity [6], [7], [10], as well as the DHF [12], [17], [18]. The multi-dimensional debris bed, e.g., the conical shape, is more realistic as the consequence of single jet release, as observed from experiments [19]. The natural circulation breaks the CCFL, so the correlations for 1D bed are not applicable. The state-of-the-art approach to evaluate the coolability of multi-dimensional debris bed is to perform numerical simulations of the

two-phase flow and boiling heat transfer for a porous particle bed defined with multi-dimensional features.

The COCOMO code, developed by IKE University of Stuttgart, is capable of modeling the thermal hydraulics of particulate debris bed under the boiling condition in the lower head or in the reactor cavity with either cylindrical or Cartesian coordinate [20]. Extensive validation works have confirmed the capability of the COCOMO code, e.g., against DEBRIS and PEARL experiments for quench phenomena, and against COOLOCE and POMECO experiments for dryout prediction [11], [20]–[22].

1.3 MELCOR code

For the safety analysis of a light water reactor (LWR), MELCOR code is one of the leading integral codes that capture the entire severe accident progression. It is developed by Sandia National Laboratory, and widely used by engineers, researchers, and regulators in many countries. The MELCOR simulation is realized by the cooperation of packages implemented with lumped parametric models, in order to achieve the high computational efficiency. Each package targets a specific accident phenomena or program control.

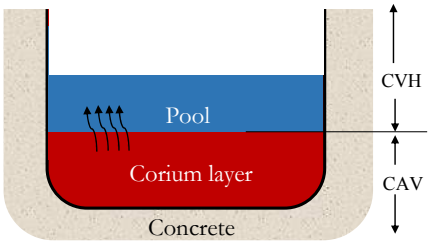

Figure 1.3 Schematic of MELCOR CAV package model.

The behavior of the corium in the cavity is modeled with the Cavity (CAV) package. The reactor cavity is considered in an axisymmetric geometry with the concrete wall retaining corium debris having one or several layers, as depicted in Figure 1.3. Each corium layer is represented with an average temperature. The energy transfer is one-dimensional. Conduction or convection models are implemented to calculate the heat transfer between the interfaces of the layers. A bounding control volume is used as the

boundary condition for the top surface of the corium. The cooling process of the corium by the pool only occurs on the top surface.

The corium layer modeled in CAV package of MELCOR is different from the porous debris bed which allows the coolant penetration to cool from inside. The features of the CAV package show that MELCOR code does not have the capability to model the coolability of ex-vessel particulate debris bed in the cavity for either quench process or DHF prediction.

1.4 Code coupling

The code coupling is an important approach to improve the simulation when the phenomena modeled by two codes are conjugated. A typical code coupling application for NPP employs a system code to calculate the response of the entire system with high efficiency, and a mechanistic code to capture the specific phenomenon of interest with high accuracy. Data communication is achieved via the coupling interface. In general, code coupling can be categorized into one-way and two-way coupling. One-way coupling means that data is transferred only from one code to the other, and it is only applicable when the physical feedback simulated from the other code is negligible. Two-way coupling means two-way data transfer between codes, which allows the two-way feedbacks, thus it has broader applications. Researches have been conducted to couple MELCOR with other codes with two-way coupling, for instance, with GASFLOW code for a detailed hydrogen distribution in containment [23], with REALAP5 code for modeling a thermosiphon loop [24], and with PECM model for modeling the molten core in the lower plenum [25].

1.5 Objectives and tasks

Motivated by the current need of safety analysis for the SAM strategy of Nordic BWRs, the ultimate goal of this thesis is to extend the capability of MELCOR code to model the ex-vessel particulate debris bed coolability, with the approach of code coupling.

The development of MELCOR capability has two major objectives in terms of the two aspects of the coolability. For the ex-vessel debris bed coolability during quench process, the coupled simulation of MELCOR and COCOMO code is developed, where the COCOMO code is in place of MELCOR CAV package. For the long-term coolability limited by the dryout condition, a fast surrogate model is developed to calculate the dryout power density of

multi-dimensional debris beds based on COCOMO prediction as full model. The implementation of the surrogate model in MELCOR is achieved by a coupling interface.

The following three main tasks are accomplished in Chapter 2, 3 and 4, respectively. Chapter 5 draws the conclusion.

- MELCOR core nodalization quantification. The effect of core mesh on the MELCOR standalone simulation for in-vessel progression is discussed, and a proper mesh to be used in the coupled simulation is selected (in Paper 1).

- MELCOR capability development by coupling: (i) with COCOMO code (in Paper 2), and (ii) with a trained surrogate model (in Paper 3).

- Application of the developed tools for the safety analysis of Nordic BWR on: (i) ex-vessel debris bed quench simulations (in Paper 2), and (ii) the long-term coolability limit predictions (in Paper 3).

2 MELCOR standalone simulation

Even though models for ex-vessel particulate debris bed cooling are absent in the code, MELCOR predictions on the in-vessel corium behavior, vessel failure and corium release could provide important preconditions for the consequent phenomena, i.e., debris bed formation and cooling. The in-vessel phenomena simulated by MELCOR is achieved by the COR package, based on a two-dimensional core nodalization. This chapter is motivated by the concern that the core mesh may influence the prediction of in-vessel phenomena and corium release.

In this chapter, the models implemented in COR package are briefly introduced. MELCOR simulations are performed for postulated severe accidents of a reference Nordic BWR, with three developed core meshes to investigate their effects. This chapter is included in Paper 1.

2.1 MELCOR models of COR package

The core mesh of the COR package is axisymmetric, which covers core and lower plenum regions with radial rings and axial levels. Three developed core meshes for the Nordic BWR are shown in Figure 2.1. The intersect of these rings and levels with the semi-spherical lower head generates the nodalization of the lower head. The number of rings and levels are decided by users. The decisions on the number and location of the rings and levels involve further considerations of the real structure inside the vessel, axial and radial power distribution and burn-up zones, etc. [26]. According to MELCOR user guide, 3 or 4 rings and 10 to 15 levels are enough for a base case nodalization of a simple full reactor plant model [27].

Each core component is represented by one equilibrium temperature in each mesh cell, no matter how large the cell volume is. The models for the in-vessel accident progression are sensitive to the core component temperature and the cell volume, as introduced briefly in the following.

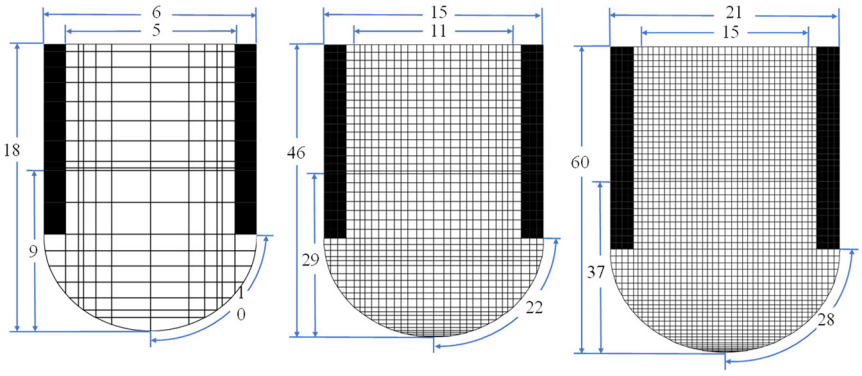

(a) 6-ring mesh (b) 15-ring mesh (c) 21-ring mesh

Figure 2.1 Two-dimensional core nodalization.

Core degradation models

During core heat-up in a postulated accident scenario, cladding failure is assumed if cell temperature is higher than a criterion temperature, which is 1173K by default. Cladding failure triggers the release of radionuclides in the fuel-cladding gap, so called “gap release”. Cladding material Zircaloy starts to melt at a default temperature of 2098K. Molten Zircaloy flows downward and freezes subsequently when it gets cooler. This process is called “candling” in MELCOR. Molten Zircaloy is held up within its oxide shell until breach occurs at a default temperature of 2400K. Oxidized fuel rods collapse based on the time-at-temperature model. Once the supporting plate of a radial ring is failed, all core materials located in that ring collapse immediately.

Core relocation models

The core relocation models are purely parametric and not based on momentum balance. The downward relocation of core material is modeled as a constant velocity movement in MELCOR. The downward relocation in each ring is treated independently for gravitational settling. The lowest core cell that core material can fill into is decided first. The filling to the lowest cell ends when the cell volume is full or the source cell is exhausted.

During the candling process of molten materials, the flow channels can be blocked by the refrozen material, which obstructs the downward relocation of molten materials. The flow blockage model in MELCOR tracks the

vertical distribution of refrozen material within a core cell, as shown in Figure 2.2. Ten sub nodes are assumed for each core cell by default. If any sub node is completely filled, blockage is formed in this cell.

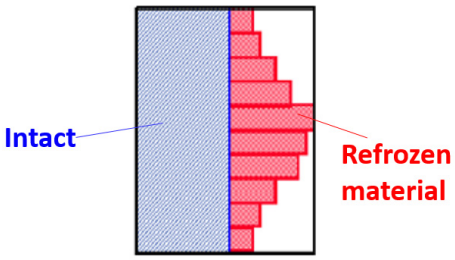

Figure 2.2 Schematic for flow blockage in a cell [27].

For the radial relocation, the possible adjacent radial rings that core material can fill into is found due to unequal level. The total volume of core material that must be moved to balance the unequal level is calculated first. Within each core time step, the volume that moves between two rings is proportional to the total volume.

From the models, it would be expected that a finer core mesh could capture higher resolution of the temperature distribution, which might affect the core degradation. The smaller cell volume in a finer core mesh might affect the core relocation and flow blockages. In order to figure out how much the accident progression could be influenced, three core mesh are developed for the Nordic BWR, as shown in Figure 2.1. The 6-ring mesh is a common one to model a full reactor by MELCOR users. The 15-ring and 21-ring mesh are finer, and barely used in other researches.

2.2 Simulation of Nordic BWR

A MELCOR input for the Nordic BWR was originally developed with the aim for the safety analysis of specific limiting transients and accidents during reactor power upgrading [28]. This input was further developed into a higher MELCOR version 2.2 in the present study, with three core mesh schemes.

The Nordic BWR has full thermal power of 3900MW during normal operation. It is equipped with multiple safety systems including the reactor scram, emergency core cooling systems (ECCS), pressure relief and

condensation system, and containment spray systems etc. [29]. In our MELCOR model, the severe accident of the Nordic BWR is assumed to be initiated by (i) station blackout (SBO); and (ii) SBO combined with a large break loss-of-coolant accident (LOCA) at the main steam line. The reactor scram is triggered with full insertion of control rods to achieve the reactor shutdown. Some active safety systems are considered unavailable due to the common case of power off, including both high-pressure and low-pressure injection of ECCS and the containment spray.

2.2.1 Nodalization

The thermal hydraulic nodalization of the Nordic BWR containment is shown in Figure 2.3. The lower drywell is a cylindrical chamber, which serves as the reactor cavity. The wetwell is an annular chamber with a deep water pool during normal operations. The containment has an inherently passive design for the pressure suppression. The water pool is used to condensate steam from the primary system either by release through the Automatic Depressurization System (ADS) (FL314) or by leaking to the drywell through the blowdown pipes (CV230 and CV240). A flow path (FL205) is used to connect the lower drywell and the wetwell, and it is assumed to be opened at the early phase of the accident.

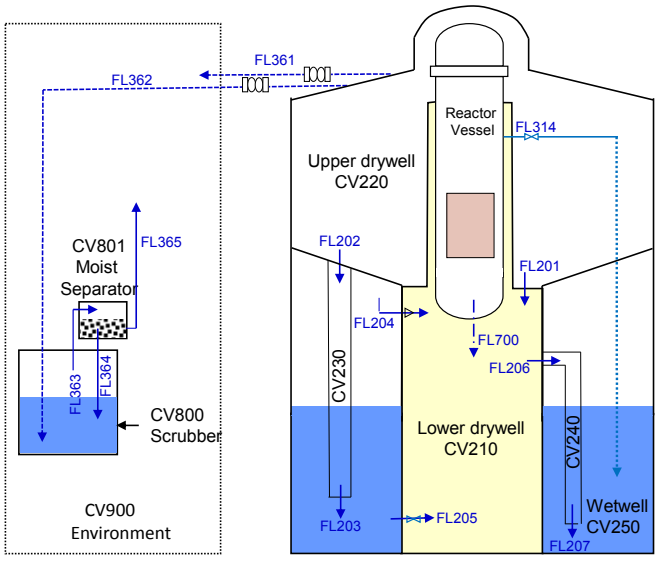

Figure 2.3 Nordic BWR containment nodalization.

The vessel is divided into several major control volumes, as shown in Figure 2.4, of which the control volumes in the core region and the lower plenum are interlinked with the core meshes.

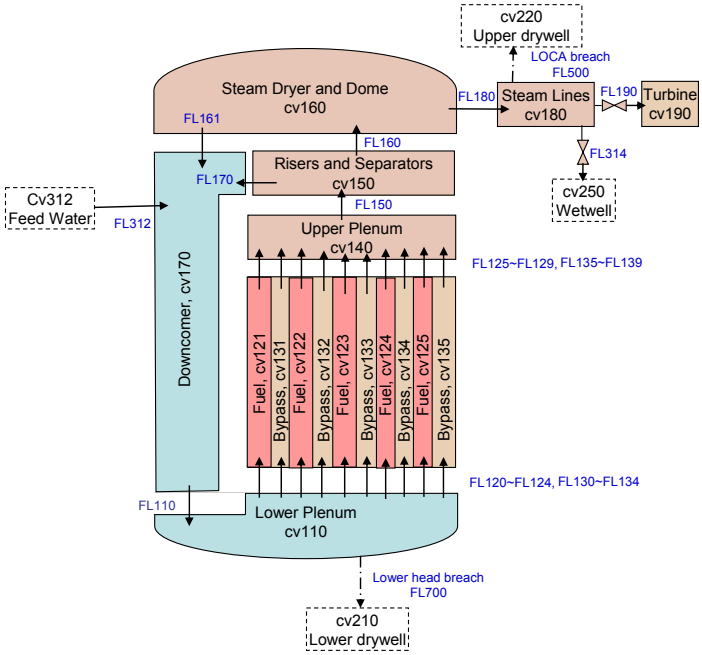

Figure 2.4 Nordic BWR in-vessel nodalization.

2.2.2 In-vessel accident progression

The severe accident progression of Nordic BWR is simulated with MELCOR version 2.2 revision 9541. The SBO scenarios simulated with the 6-ring, 15-ring and 21-ring core meshes are named as SBO-6, SBO-15 and SBO-21, respectively. Similarly, the SBO+LOCA scenarios are named as LOCA-6, LOCA-15 and LOCA-21.

The timelines for main events are plotted in Figure 2.5. During the early phase of the SBO scenario, the in-vessel coolant level drops due to insufficient coolant supply. Low water level triggers the activation of ADS and lower drywell flooding. Fuel rods start to heat up when they are uncovered by coolant. Gap release indicates the start of core degradation. The failure of core support plate indicates the start of core relocation to the

lower plenum. Simulated by the Larson-Miller creep rupture model [30], the vessel breach is predicted, which leads to the corium release into cavity pool. Containment venting is activated when the containment pressure reaches the designed critical value. For the SBO+LOCA scenario, the breach at the main steam line connects the vessel and containment drywell directly, and causes a quick depressurization of the vessel. It accelerates coolant vaporization in vessel and leads to a faster accident progression at the early phase and an earlier containment venting time.

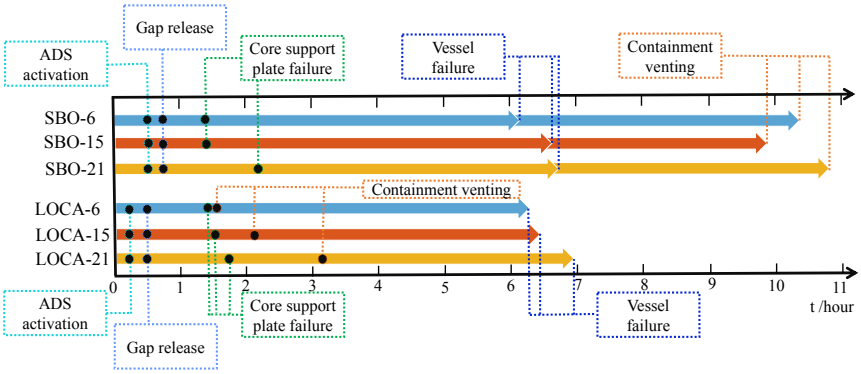

Figure 2.5 Accident progression for different cases.

Comparing the predictions from three core meshes, the time to reach the ADS activation and gap release has little difference. Later when core degradation and relocation start, the time difference becomes apparent. The core support plate failure time, vessel failure time and containment venting time are generally delayed with finer meshes for both SBO and LOCA scenarios.

The visualization of the in-vessel core degradation and relocation for SBO scenario is plotted in Figure 2.6 ~ Figure 2.8. The first row in each figure table is drawn by Symbolic Nuclear Analysis Package (SNAP) for volumetric distribution of core component, and the second row in each figure table is drawn by MATLAB to show the maximum temperature distribution in each mesh cell. The color for component and color bar for temperature scale are illustrated in Figure 2.9.

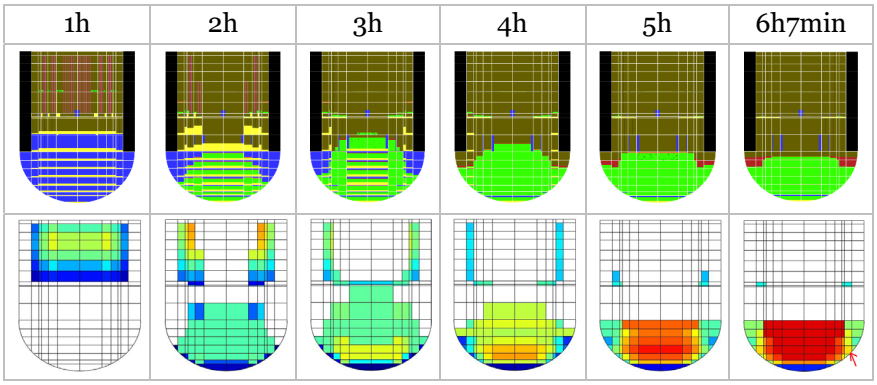

Figure 2.6 Volume and temperature distribution for SBO-6 case.

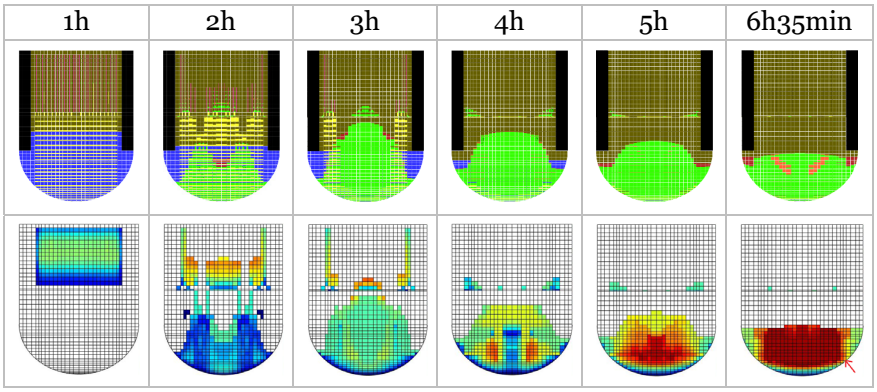

Figure 2.7 Volume and temperature distribution for SBO-15case.

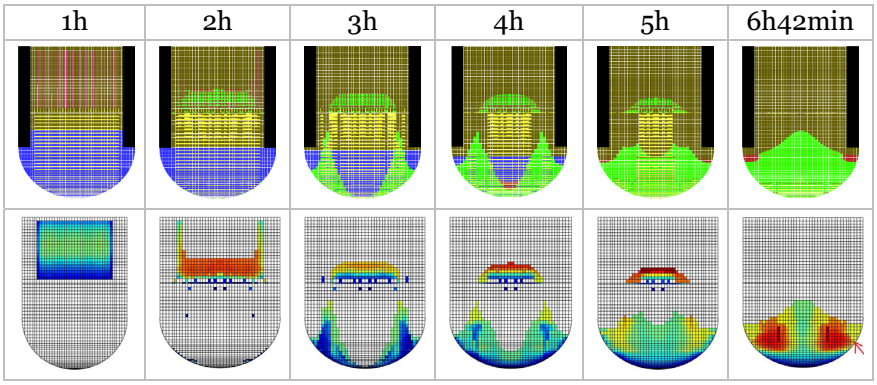

Figure 2.8 Volume and temperature distribution for SBO-21case.

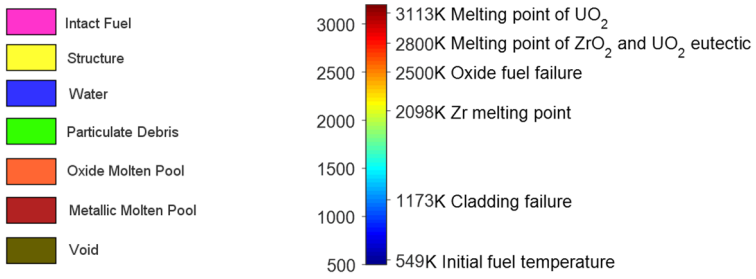

(a) component (b) temperature

Figure 2.9 Color illustration.

The visualization figures show two major effects. The first effect is the different sequences of core support failure location. For SBO-6 case, core support plate starts to fail from the central ring. For SBO-15 case, the plate fails from the middle ring. While for SBO-21 case, the plate fails from the outermost ring. The reason is probably related to the flow blockage model of MELCOR. The finer meshes tend to have smaller cell volume in the central rings above core plate, which leads to more intense formation of the flow blockage in these cells. The local blockage in these cells obstructs downward-relocating molten materials, thus hinders the core plate heated by the falling corium in central rings.

The second effect is about the in-vessel debris bed located in the lower plenum. It is found that finer mesh cases tend to have longer existence of the heap in the lower plenum. The possible reason is due to the mesh-based parametrical radial relocation model of MELCOR. The volume of debris that moves between adjacent rings within one core timestep is proportional to cell volume. Larger cell volume in coarse meshes allow large volume movement within one core timestep, which promotes the levelling off. Besides, coarse meshes have less rings and levels, which cannot capture the shape as accurately as finer meshes do.

The gross failure of the lower head leads to a fast discharge of the corium from vessel to cavity. The amount of the released corium mass is shown in Figure 2.10. For SBO-6 case, two thirds of the corium mass inside vessel is released within 20min after vessel failure occurs, and the release of all corium mass takes less than 2h. Finer mesh cases tend to take longer time, and have a little more corium release. The extra corium mass is due to the more oxidation of the metallic component of the core material.

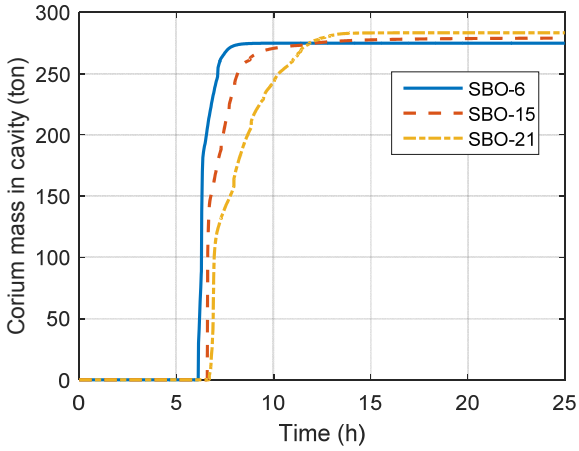

Figure 2.10 Corium mass relocated from vessel into the cavity.

2.3 Summary

This chapter discusses the effect of MELCOR core mesh on the predictions of in-vessel accident phenomena, vessel failure and corium release, which are the preconditions for debris bed formation. It is found that for the Nordic BWR, the effect on core plate failure sequence and the debris relocation in lower plenum is distinguished. The coarse mesh case tends to lead to an earlier vessel failure time and a faster corium release, which makes it most conservative for the subsequent ex-vessel debris bed cooling, since the earlier formation of debris bed means a higher decay power. Therefore, the following MELCOR coupled analysis on the debris bed coolability uses the 6-ring core mesh, which is also advantageous due to its higher computational efficiency compared with finer core meshes.

3 Development of MELCOR coupled simulation

In this chapter, the MELCOR capability on modeling ex-vessel debris bed coolability is extended by code coupling with COCOMO code and a surrogate model, separately. The coupling with COCOMO code is included in Paper 2. The development of the surrogate model is included in Paper 3.

3.1 Coupling with COCOMO code

3.1.1 COCOMO models

In COCOMO code, the particulate debris bed is considered as a fixed matrix of high-permeability porous medium with user-defined geometry, particle diameter and porosity in either cylindrical or Cartesian coordinate. The coolant in either liquid or gas phase could enter in the void zones of the porous media.

Mass equations

The mass balance is considered for coolant in liquid and gas phase, as listed in Eq. (3.1) and (3.2).

Liquid:
$$\frac{\partial}{\partial t}\varepsilon s\rho_l + \nabla\cdot(\varepsilon s\rho_l\overrightarrow{v_l}) = -\Gamma^{evap} \tag{3.1}$$

Gas:
$$\frac{\partial}{\partial t}\varepsilon(1-s)\rho_g + \nabla\cdot\left[\varepsilon(1-s)\rho_g\overrightarrow{v_g}\right] = \Gamma^{evap} \tag{3.2}$$

Γ^{evap} is the mass transfer rate due to evaporation or condensation.

Momentum equations

The momentum equations for coolant in liquid and gas phase are listed in Eq. (3.3) and (3.4). They are simplified by neglecting the inertial terms for

both temporal and spatial derivatives of the velocities. The dominating forces in the equations from left to right are (i) the friction forces between fluids and solid particles; (ii) the interfacial drag between liquid and gas phase; (iii) pressure gradient; and (iv) buoyancy force.

Liquid: $$K_{l,s}\vec{v}_l + \frac{K_{g,l}}{s}\left(\vec{v}_g - \vec{v}_l\right) = -\nabla p_l + \rho_l \vec{g} \tag{3.3}$$

Gas: $$K_{g,s}\vec{v}_g + \frac{K_{g,l}}{(1-s)}\left(v_g - \vec{v}_l\right) = -\nabla p_g + \rho_g \vec{g} \tag{3.4}$$

For friction coefficient $K_{l,s}$ $K_{g,s}$ and interfacial drag coefficient $K_{g,l}$, several friction models are implemented in the COCOMO code. The friction coefficients for two-phase flow in porous media are extended from the single-phase friction law of the Ergun equation [31], by introducing relative permeability κ_r and relative passability η_r. The friction coefficients have a general form as follows:

$$K_{l,s} = \frac{\mu_l}{\kappa\kappa_{r,l}} + \frac{\rho_l}{\eta\eta_{r,l}}|\overrightarrow{v_l}| \tag{3.5}$$

$$K_{g,s} = \frac{\mu_g}{\kappa\kappa_{r,g}} + \frac{\rho_g}{\eta\eta_{r,g}}\left|\overrightarrow{v_g}\right| \tag{3.6}$$

The permeability κ and passability η for single-phase are correlated based on experiments measured for a variety of fluids and granular sands:

$$\kappa = \frac{\varepsilon^3 d^2}{150(1-\varepsilon)^2} \tag{3.7}$$

$$\eta = \frac{\varepsilon^3 d}{1.75(1-\varepsilon)} \tag{3.8}$$

The relative permeability and passability for liquid and gas phases are expressed as functions of the saturation [32].

$$\kappa_{r,l} = s^n,\ \eta_{r,l} = s^m \tag{3.9}$$

$$\kappa_{r,g} = (1-s)^n,\ \eta_{r,g} = (1-s)^m \tag{3.10}$$

The classic models, including Lipinski model [33], Reed model [34], and Hu & Theofanous model [12], are correlated from their own experimental

data and have different values of the empirical constants n and m, where n = 3 (all three models) and m = 3 (Lipinski), or 5 (Reed), or 6 (Hu & Theofanous). These classical models do not explicitly consider the interfacial drag between liquid and gas.

Besides classical models, three models are implemented with the explicit consideration of the interfacial drag. Schulenberg & Müller model was proposed to correlate the interfacial drag as an expression of buoyancy, viscous force, inertial and capillary force, fitting from their experimental data [35]. Tung & Dhir model was developed theoretically to account for the particle-gas drag, particle-liquid drag and liquid-gas interfacial drag within three flow regimes [36]. Due to the over-prediction of Tung & Dhir model on the friction of a particulate beds packed with smaller particles, e.g., 5.8mm in diameter, a modified Tung & Dhir model (MTD model) was proposed in order to extend its applicability on small particles [37]. Detailed equations of these three models can be found in [38].

Energy equations

The energy equations for coolant in gas phase and liquid phase, and for solid particles are listed in the following equations.

Liquid: $$\frac{\partial}{\partial t}\varepsilon s\rho_l e_l + \nabla\cdot(\varepsilon s\rho_l \overrightarrow{v_l} i_l) = \nabla\cdot\left(k_l^{eff}\nabla T_l\right) + Q_{s,l} - Q_{l,sat} - \Gamma^{evap} i_{l,sat} \quad (3.11)$$

Gas: $$\frac{\partial}{\partial t}\varepsilon(1-s)\rho_g e_g + \nabla\cdot\left(\varepsilon(1-s)\rho_g \overrightarrow{v_g} i_g\right) = \nabla\cdot\left(k_g^{eff}\nabla T_g\right) + Q_{s,g} - Q_{g,sat} + \Gamma^{evap} i_{g,sat} \quad (3.12)$$

Solid: $$\frac{\partial}{\partial t}\rho_s e_s = \nabla\left(k_s^{eff}\nabla T_s\right) + Q_s^{Decay} - Q_{s,g} - Q_{s,l} \quad (3.13)$$

Figure 3.1 shows the schematic of heat transfer process modeled in COCOMO code. The correlations to calculate the heat transfer coefficients are listed in Table 3.1. $Q_{s,l}$ represents the heat flux between solid and liquid, when the surrounding bulk is liquid, and the temperature of the solid particles T_s is below the saturation temperature T_{sat}. Correspondingly, $Q_{s,g}$ represents the heat flux between solid and gas, when the surrounding bulk is gas, and T_s is above T_{sat}. The boiling heat flux $Q_{s,sat}$ is considered in three regimes:

(i) pool boiling regime when $T_s \leq T_{min}^{FB}$;

(ii) transition regime when $T_{min}^{FB} < T_s < T_{max}^{PB}$; and

(iii) film boiling regime when $T_s \geq T_{max}^{PB}$.

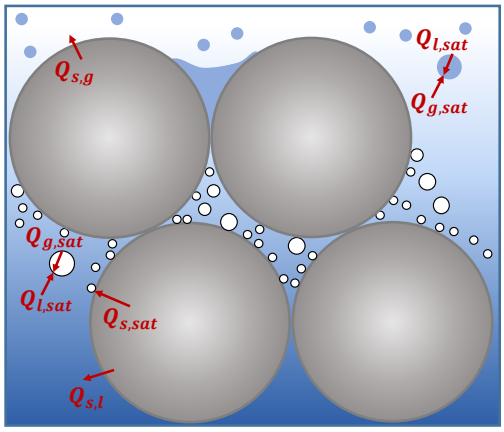

Figure 3.1 Schematic of heat transfer between solid, liquid and gas phase.

The minimum film boiling temperature is defined as $T_{min}^{FB} = T_{sat} + 17K$, and the maximum pool boiling temperature is defined as $T_{max}^{PB} = T_{min}^{FB} + 100K$. In the transition zone, the heat transfer coefficient is obtained by linear interpolation.

For the heat transfer between interface and liquid or gas bulk, it is considered into three regimes based on the liquid fraction, denoted by s. By default:

(i) $s \geq 0.7$: liquid phase is continuous and in bubbly flow;

(ii) $s \leq 0.3$: gas phase is continuous and in droplet flow; and

(iii) $0.3 < s < 0.7$: bubbly flow and droplet co-exist, and the heat transfer coefficient is weighted by the liquid fraction.

Table 3.1 Heat transfer correlations

Heat flux	Correlations
$Q_{s,l}$	Satisfy both: (i) $T_s < T_{sat}$; (ii) liquid is continuous $Nu_{s,l} = 2 + 0.6Re_l^{1/2}Pr_l^{1/3}$
$Q_{s,g}$	Satisfy both: (i) $T_s > T_{sat}$; (ii) gas is continuous $Nu_{s,g} = 2 + 0.6Re_g^{1/2}Pr_g^{1/3}$
$Q_{s,sat}$	Pool boiling $T_s \le T_{min}^{FB}$: $T_{min}^{FB} = T_{sat} + 17K$ $h_{s,sat}^{PB} = \frac{c_{p,l}^3 \cdot \mu_l \cdot (T_s - T_{sat})^2}{(i_{g,sat} - i_{l,sat})^2 \cdot (0.012Pr_l)^3 \cdot \sqrt{\frac{\sigma_l}{g(\rho_l - \rho_g)}}}$
	Film boiling $T_s \ge T_{max}^{PB}$: $T_{max}^{PB} = T_{min}^{FB} + 100K$ $Nu_{l,sat}^{FB} = 0.67 \cdot \left(\frac{\rho_g \cdot g \cdot (\rho_l - \rho_g) \cdot \Delta i'_{sat} \cdot d^3}{\mu_g \cdot k_g \cdot (T_s - T_{sat})}\right)^{1/4}$ where modified latent heat: $\Delta i'_{sat} = (i_{g,sat} - i_{l,sat}) \cdot \left[1 + \left(0.968 - \frac{0.163}{Pr_g}\right) \cdot Ja\right]$ $Ja = \frac{c_{p,g} \cdot (T_s - T_{sat})}{i_{g,sat} - i_{l,sat}}$
	Transition region $T_{min}^{FB} < T_s < T_{max}^{PB}$: $h_{s,sat}^{trans} = [1 - W(T_s)] \cdot h_{s,sat}^{PB}(T_{min}^{FB}) + W(T_s) \cdot h_{s,sat}^{FB}(T_{max}^{PB})$ $W(T_s) = \frac{T_s - T_{min}^{FB}}{T_{max}^{PB} - T_{min}^{FB}}$
$Q_{l,sat}$	Bubbly flow: $Nu_{l,sat}^{B} = 2 + 0.6Re_{l,rel}^{1/2}Pr_l^{1/3}$
	Droplet flow: $Nu_{l,sat}^{D} = 10$
$Q_{g,sat}$	Bubbly flow: $Nu_{g,sat}^{B} = 10$
	Droplet flow: $Nu_{g,sat}^{D} = 2 + 0.738Re_{g,rel}^{1/2}Pr_g^{1/3}$

3.1.2 Simulation settings

Figure 3.2 shows an axisymmetric computational domain of COCOMO simulation. The debris bed is assumed to be conical, which is a probable shape as a result of single axisymmetric jet released from the vessel bottom. The properties of the debris bed should be defined, including the geometry, the porosity, the particle size and the power density. The upper boundary is treated as an open boundary with defined pressure. The initial conditions require the temperature and the pressure of the cavity pool, and the temperature of the debris bed.

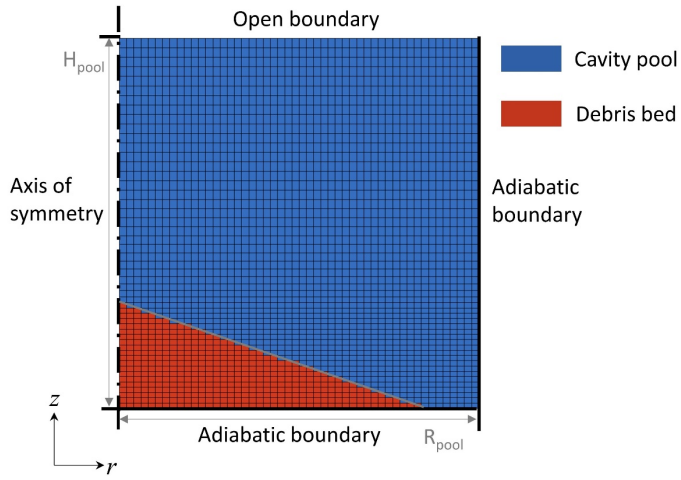

Figure 3.2 Simulation domain of COCOMO.

For the selection of friction model, several validation studies are taken into account. The validation against the pressure gradient in POMECO-FL and Tutu experiments indicates that both Reed model and MTD model are capable. The validation against dryout experiments without downcomer shows the Reed model could well produce the dryout values and locations. The Schulenberg & Müller model works better for the homogenous bed with downcomer. Because the wall friction is not modeled, the Reed model could trade off the wall friction by its under-estimation of the frictions [11]. The validation against the quench experiment shows that the quench process is predicted faster with MTD model than Reed model. It is because the upward steam flow would accelerate the liquid coolant when

considering the interfacial drag with the MTD model, then the liquid penetration in the bed would be promoted [22]. From a conservative point of view, the Reed model is selected for the following investigations.

3.1.3 MELCOR/COCOMO coupling interface

The left plot in Figure 3.3 shows the MELCOR nodalization of the Nordic BWR containment with the lower drywell already flooded into a deep water pool. The right plot shows the schematic of COCOMO computational domain. COCOMO simulates the cooling of the debris bed in the lower drywell pool in place of the MELCOR CAV package.

During coupled simulation, MELCOR provides the pressure and the pool temperature to COCOMO as the initial and boundary conditions, and the decay power as the heat source of the debris bed. COCOMO calculates the boiling heat transfer from particles to the pool and provides the heat transfer rate to MELCOR as the energy source of the pool.

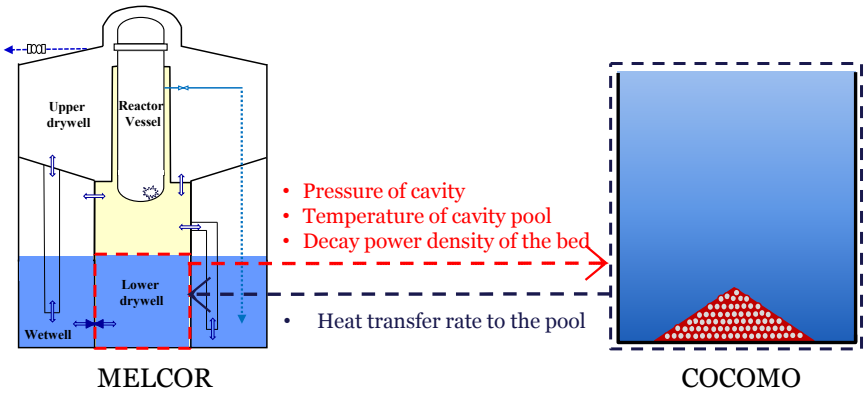

Figure 3.3 Computational domain and data exchange for MELCOR /COCOMO coupling.

The coupling interface requires a communication program MPIEXEC and an external coupling program DINAMO, as their relationship shown in Figure 3.4. MPIEXEC program controls the MELCOR execution and coordinates the data exchange [23]. DINAMO (Direct Interface for Adding Models) program, developed by KIT, is aimed to couple new models to MELCOR code [25]. DINAMO program serves as a platform, of which one side communicates with MELCOR via the MPIEXEC program, and the

other side communicates with the coupled code or program. The coupling interface of MELCOR/COCOMO is achieved by integrating the source codes of DINAMO and COCOMO together to build a new executable. The data exchange from the coupling interface to the COCOMO side could be accomplished internally and fast.

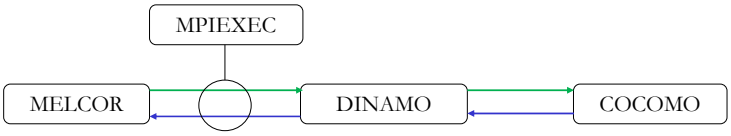

Figure 3.4 The coupling interface of MELCOR/COCOMO.

Figure 3.5 shows the synchronization logic for data exchange between two codes. The horizontal axes represent the calculation time advancement of two codes. The number above or below the intervals of the time axis denotes the order of the advancing steps during the coupled calculation. An asynchronous time advance is used. To be specific, MELCOR first starts the simulation of the severe accident progression from reactor scram. When vessel failure is predicted, MELCOR sends data to COCOMO for initialization. MELCOR runs for one time step with time interval 1, and it suspends. COCOMO then starts the simulation for several time steps (i.e. time interval 2~5 in the figure), until two codes meet at the same time point. Two codes exchange data and proceed for the next cycle.

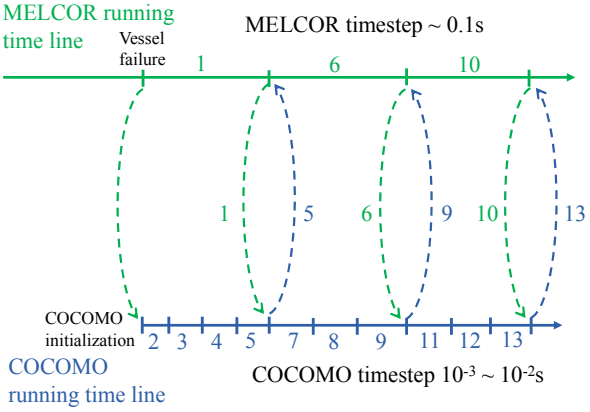

Figure 3.5 Synchronization logic for data exchange.

3.2 Coupling with a surrogate model

The Lipinski 0-D correlation is implemented in MELCOR code to calculate the dryout heat flux as a limiting maximum heat transfer rate of an in-vessel particulate debris bed. It is proposed for 1D debris bed, not applicable for the multi-dimensional debris bed.

The dryout of a multi-dimensional debris bed could be predicted by the numerical simulation of COCOMO code. To perform it in COCOMO, a thermal equilibrium state between the bed and the saturated pool is assumed as the initial condition. The dryout condition is found by gradually increasing of the debris bed power until the local temperature of the bed jumps much higher than the saturation temperature. Each attempt requires the code to run once. The simulation process is computationally costly, and cannot be used by other codes like MELCOR or a probabilistic safety analysis (PSA).

To address this issue, a surrogate model is developed to substitute the full model, which is the numerical solving process by COCOMO simulation. A surrogate model is able to approximate the full model based on limited samples, when the full model cannot be used because it is either a black box or computationally unaffordable.

The DHF for a 1D bed is defined as the dryout power divided by the cross-section area, which is not suitable for a multi-dimensional bed because the cross-section area varies with bed height. The mass-averaged dryout power density, defined as the dryout power divided by the total mass, is therefore employed. For convenience, the following mentioned “dryout power density” is mass-averaged.

3.2.1 A surrogate model for dryout

The surrogate model is aimed to predict the dryout power density of a debris bed with an 2D axisymmetric geometry, e.g. the debris bed A, B and C shown in Figure 3.6. The homogenous particle size and porosity is assumed preliminarily.

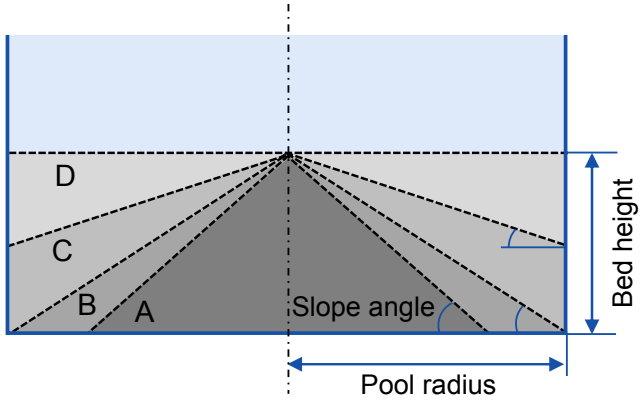

Figure 3.6 Multi-dimensional debris beds with the same height.

Surrogate model output

Four debris beds (A to D) in Figure 3.6 have the same bed height but different slope angle. A characteristic factor is proposed to correlate the multi-dimensional debris bed (A to C) with the one-dimensional debris bed (D). Specifically, the dryout power density of the bed A and D, denoted by q'_A and q'_D, are correlated by the characteristic factor f_A as:

$$q'_A = f_A \times q'_D \tag{3.14}$$

q'_D can be quickly estimated by the Lipinski 0-D model. Thus, the characteristic factor can be calculated by the full model as:

$$f_{A,FM} = \frac{q'_{A,COCOMO}}{q'_{D,Lipinski}} \tag{3.15}$$

If the surrogate model is trained for the characteristic factor, then the dryout power density of the debris bed A could be quickly estimated as:

$$q'_{A,SM} = f_{A,SM} \times q'_{D,Lipinski} \tag{3.16}$$

The output of the surrogate model is turned into the characteristic factor, instead of the dryout power density directly.

Surrogate model inputs

The input parameters should include user-defined parameters in the full model for determining the unique debris bed with initial and boundary

conditions. The input parameters are mainly considered from two aspects: (i) the debris bed properties, and (ii) the pool condition.

The bed properties include the porosity, the particle size, and the geometry. The particle diameter is used to quantify the particle size, since the particles are considered as spherical. In order to determine the unique geometry of the axisymmetric debris bed in Figure 3.6, it requires the height and the slope angle of the bed, and the radius of the cavity pool. The slope angle and the radius of the cavity are considered as independent input parameters. In addition, the total bed mass is considered as independent instead of the bed height. The total bed mass, as a consequence of corium release from the vessel, could be predicted from other simulation like MELCOR or engineering judgement.

A saturated pool is considered as an initial condition and the bed is at the pool temperature initially. The saturation temperature of the pool is determined by the ambient pressure, which is served as the boundary condition. Therefore, the ambient pressure is considered as an independent input parameter for the surrogate model.

To sum up, six parameters are considered as the input parameters of the surrogate model, including porosity, particle diameter, debris bed total mass, slope angle, cavity radius, and ambient pressure. The ranges for these parameters are discussed below, and summarized in Table 3.2.

Porosity: The theoretical minimum porosity for the porosity of a particulate bed with homogenous spherical particles is around 0.36. However, for a prototypical debris bed with irregular shape of particles, the porosity would be uncertain. The packed particulate beds in dryout experiments are compact with small measured porosity, e.g. POMECO tests: 0.29~0.41 [39], and COOLOCE tests: 0.375~0.4 [40]. The formed particulate beds from jet fragmentation experiments have larger porosity e.g. CCM tests: 0.53~0.68 [41], and DEFOR tests: 0.57~0.71 [42]. A relatively large range of porosity 0.3 to 0.7 is selected, in order to cover possible scenarios.

Particle diameter: The particle size sieved from the jet fragmentation experiment FARO tests was in millimeter scale, distributed from 0.25 mm to 11 mm [3]. The concept of the effective particle diameter has been proposed, which employs one diameter representing the complex particle size of the debris bed, and satisfying the simulation of the pressure drop or the dryout. Recent study reveals that the effective diameter is relevant to

the bed configuration, which makes it difficult to find a unified formula. In a dryout prediction test, the effective diameter was quantified to be lower than the Sauter mean diameter (surface-average diameter) [43]. The range of the effective particle diameter considered in the present study is wide from 0.5 mm to 10.0 mm.

Debris bed mass: The range for the total mass of the debris bed is considered from 50 tons to 350 tons, which is large enough to cover the worst scenario of the release of all in-vessel corium for Nordic BWR.

Slope angle: The one-dimensional debris bed has the minimum slope angle of 0°. The maximum slope angle for a conical particulate bed is defined as the critical angle of repose. There is currently no experimental evidence for the critical angle of repose of the prototypical particulate debris bed. A previous study considers an uncertain range of (22°, 35°) for the critical angle of repose of debris bed [44]. From a conservative point of view, 45° is considered as the maximum slope angle in this study, in order to provide a large range for user choices.

Cavity radius: The range of cavity radius is considered from 4.5 m to 6.5 m. The cavity of Nordic BWR is 6.1 m.

Pool ambient pressure: For Nordic BWR, the ambient pressure of the cavity pool can be considered as the containment pressure. In this study, the maximum value of the pressure is considered as 10 bar, in order to be feasible for more reactor applications.

Table 3.2 Input parameter ranges of the surrogate model in respect to debris bed and system properties

Parameter	Minimum value	Maximum value
Porosity	0.3	0.7
Particle diameter (mm)	0.5	10.0
Debris bed mass (ton)	50.0	350.0
Slope angle (°)	0.0	45.0
Cavity radius (m)	4.5	6.5
Pool ambient pressure (bar)	1.0	10.0

Surrogate model training

A sample size of 400 cases is generated, and each case represents a group of input parameters sampled from their range. Each case is simulated with COCOMO code to predict the dryout power density. The dryout power density of the corresponding one-dimensional debris bed for each case is also calculated with Lipinski 0-D model. The characteristic factor from the full model prediction is obtained for all sampled cases.

The surrogate model for the characteristic factor is trained with Kriging approach using the open-source Python package: surrogate modeling toolbox (SMT) [45]. Kriging surrogate model is created based on sparsely sampled data, and the response on a new point can be estimated.

One quarter of the sample cases are randomly selected to train the surrogate model. The rest samples are used to test the accuracy of the surrogate model. Figure 3.7 (a) and (b) show the comparison between surrogate model and full model for the characteristic factor and the dryout power density, respectively. The prediction error is within ±10%, which shows a good agreement. The characteristic factor is generally larger than 1 and less than 2 in Figure 3.7 (a), which means the dryout power density of the multi-dimensional debris bed is greater than the corresponding 1D debris bed with the same height, but less than 2 times. It should be noted that it is based on the COCOMO and Lipinski model simulation and sparsely sampled cases, instead of observations from experiments.

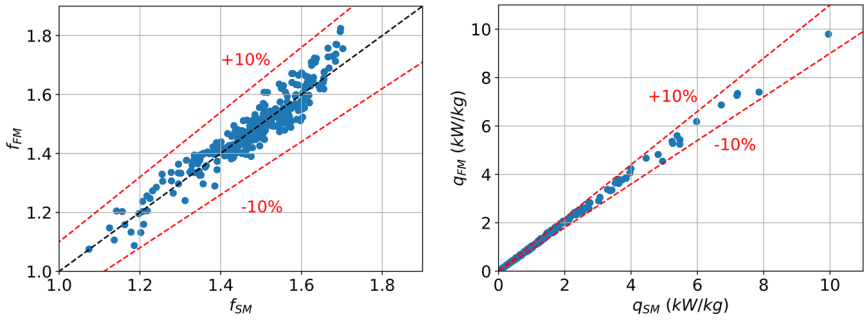

(a) Characteristic factor (b) Dryout power density

Figure 3.7 Comparison between surrogate model and full model.

In order to quantify the accuracy of the surrogate model, the ratio of the predictions between the surrogate model and the full model is plotted in Figure 3.8. The probabilistic density function (PDF) of the ratio could be fitted into a Normal distribution $N(0.999, 0.027)$, which could be treated as a model uncertainty.

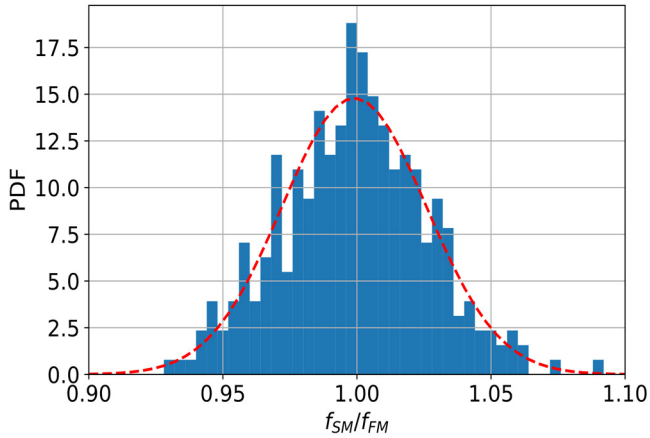

Figure 3.8 PDF for the ratio of surrogate model over full model.

3.2.2 Coupling interface between MELCOR and surrogate model

With the help of the coupling interface, the dryout power density predicted by the surrogate model can be returned to MELCOR, as the schematic shown in Figure 3.9. After the vessel failure predicted by MELCOR, the data from the MELCOR simulation, including the cavity pressure and the corium mass ejected from the vessel, are sent to DINAMO. DINAMO writes them into an external file for the surrogate model to read. Other input e.g. porosity, particle diameter, and slope angle should be defined by users. The output of the surrogate model is written into an external file for DINAMO to read. The dryout power density is returned to MELCOR as a control function value in each time advance of MELCOR.

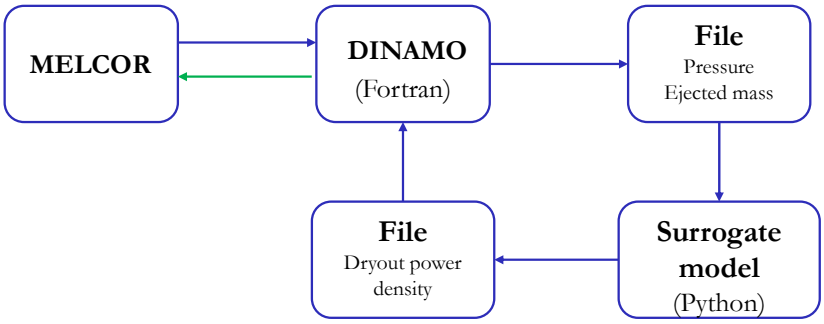

Figure 3.9 Interface for coupling between MELCOR and surrogate model.

3.3 Summary

The MELCOR capability on debris bed coolability has been extended with the code coupling approach in two aspects.

The coupling of MELCOR and COCOMO is achieved. The COCOMO code is in place of MELCOR CAV package to perform the numerical simulation of a particulate debris bed cooling in a cavity pool. The coupled simulation is suitable for the investigation of ex-vessel debris bed quench under prototypical condition.

A surrogate model is trained based on COCOMO code as full model to predict the dryout power density of a multi-dimensional debris bed. It is coupled with MELCOR for the evaluation of the debris bed long-term coolability.

4 Application to safety analysis

In this chapter, the developed simulation tools are implemented in the severe accident safety analysis for Nordic BWR. The debris bed quench simulation is included in Paper 2. The long-term coolability prediction is included in Paper 3.

4.1 Debris bed quench

The MELCOR/COCOMO coupled simulation is used to investigate the ex-vessel debris bed being quenched in the lower drywell pool under prototypical condition. As a preliminary study, the oxidation of the metallic debris and re-melting are not considered.

The initial temperature of the debris bed is essential for the quench process simulation. In the present study, the initial temperature of the debris bed is assumed as an averaged temperature based on the MELCOR prediction of the debris energy. The energy of the debris bed is approximated by the total in-vessel corium energy at the vessel failure time subtracting the energy loss during corium settling. As a result, the initial temperature is 1854 K.

The bed properties including porosity, particle size and geometry are quite stochastic as the consequence of jet fragmentation and debris settling. Their uncertainties are discussed in Chapter 3.2.1 for the development of the surrogate model. In this chapter, the effective particle diameter and the debris bed shape are investigated. The porosity of the debris bed is assumed as 0.42, which is also used in previous works [22], [46].

It should be noted that during the coupled simulation, the MELCOR predicts a gradual release process of the corium within 30 min, while the debris bed is assumed to appear in COCOMO computational domain right after vessel failure time. This means extra energy is introduced to the system, due to the co-exist of unreleased corium inside vessel in MELCOR and the debris bed in COCOMO during the corium release time. This is the

limitation of our current simulation tool. As a preliminary study, the current simulation is conservative.

4.1.1 Effective particle diameter

The effective particle diameter of a multi-dimensional debris bed during the quench process is investigated based on that the COCOMO allows defining an inhomogeneous bed with different particle diameter in each mesh cell.

The inhomogeneous particle diameter defined in each mesh cell is sampled from the particle size distribution measured from FARO test L31 [3]. The FARO tests were aimed to investigate the corium jet breakup and fragmentation in a water pool under different conditions. The prototypical corium material was used for the jet, comprising a mixture of 80% UO_2 and 20% ZrO_2. In L31 test, a total 92 kg of the melt was released into a highly subcooled pool with the pool temperature of 291 K, and the initial system pressure of 2.2 bar. The pool condition of L31 is very similar to the Nordic BWR scenario. It was observed in L31 test that the jet was well-fragmented and a particulate debris bed was formed. The particles formed in L31 test were sieved by three layers. The distribution of particle size for each layer is plotted in Figure 4.1 with data collected from [4], and the total distribution is collected from [3]. Three layers are probably equal in mass based on rough estimation.

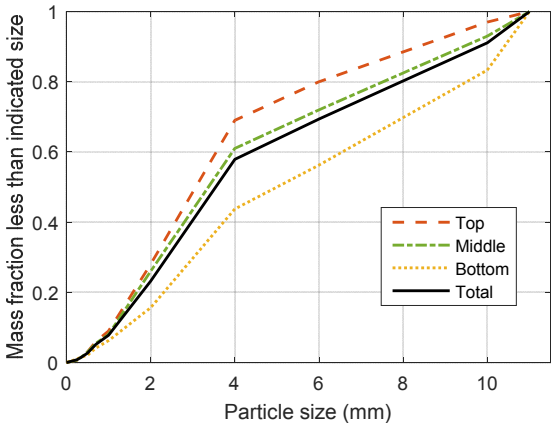

Figure 4.1 FARO L31 test particle size distribution [3], [4].

A debris bed is considered with a conical shape and slope angle of 35°, as shown in the computational domain in Figure 4.2. Three layers are divided for the debris bed, and the mesh cell in each layer is defined with a particle diameter sampled from the corresponding particle size distribution in Figure 4.1. The sampling is performed multiple times, in order to reduce the sampling error. The quench process is simulated with the MELOR/COCOMO coupled simulation for all sampled cases.

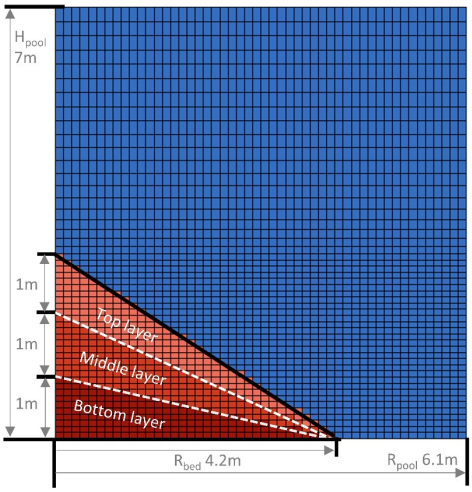

Figure 4.2 Computational domain of the debris bed.

The quench process of the inhomogeneous debris bed should be quantitatively represented by the homogeneous bed defined with the effective particle diameter. The quench rate, plotted as the quenched bed mass fraction with time, is used for the quantitative evaluation.

Four definitions of mean diameter for spherical particles are listed in Table 4.1. The surface mean diameter is also named as Sauter mean diameter. The mean diameter ranges for the sampled cases are also listed in the Table 4.1.

Table 4.1 Definitions of the mean diameter for spherical particles

Symbol	Name	Expression	Sampled cases
d_n	Count mean diameter	$\frac{\sum n_i d_i}{\sum n_i}$	0.37 ~ 0.54mm
d_l	Length mean diameter	$\frac{\sum n_i d_i^2}{\sum n_i d_i}$	0.73 ~ 1.09mm
d_s	Surface mean diameter	$\frac{\sum n_i d_i^3}{\sum n_i d_i^2}$	2.07 ~ 2.51mm
d_v	Volume mean diameter	$\frac{\sum n_i d_i^4}{\sum n_i d_i^3}$	4.36 ~ 4.80mm

Two cases with maximum and minimum mean diameter among all sampled cases are selected to show their quench rate in Figure 4.3. In each plot, it is compared with two homogenous cases defined with Sauter mean diameter and 1.1 times the Sauter diameter. The inhomogeneous case represented by the blue solid line is closer to the black dashed lines, and they even coincide partially. Quantified by the quench rate, the effective particle diameter of an inhomogeneous multi-dimensional debris bed is suggested 10% larger than the Sauter mean diameter, based the coupled MELCOR /COCOMO simulation.

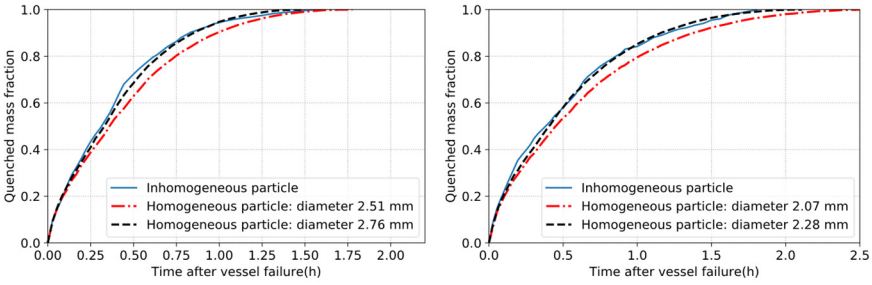

(a) Maximum mean diameter case (b) Minimum mean diameter case

Figure 4.3 Quenched mass fraction with time.

Table 4.2 lists the maximum temperature increase that the debris bed could reach during quench process, as well as the fraction of the debris bed

mass with certain temperature increases. The particle diameter of two homogenous cases is 1.1 times the maximum and minimum Sauter mean dimeter of the inhomogeneous cases, also used in Figure 4.3. The range between two homogenous cases tends to be higher than the range of the inhomogeneous cases. It indicates that the effective particle diameter using 10% larger than the Sauter mean diameter is conservative in terms of the debris bed temperature increase.

Table 4.2 Maximum temperature and debris bed mass fraction with certain temperature increases

Case		Homogenous 2.76 mm	Homogenous 2.28 mm	Inhomogeneous cases
Maximum temperature increase		505 K	684 K	429~581 K
Debris mass fraction with temperature increase	100 K	33.4%	39.5%	29.3%~37.9%
	200 K	14.5%	20.9%	10.9%~18.9%
	300 K	5.2%	10.9%	3.6%~8.0%
	400 K	1.1%	4.9%	0.3%~2.3%

4.1.2 Debris bed shape

The probable shape of the debris bed as a result of a single jet is a heap-like (conical) shape, as observed in DEFOR tests [19]. The self-leveling of the debris bed may occur due to the intense boiling of the coolant during the quench process, which may reduce the debris bed slope angle [47].

Considering the uncertainties of the slope angle and the possible self-leveling phenomena, three bed shapes are discussed as the shown in Figure 4.4. Case A and Case B have slope angle of 35° and 22°, which are the maximum and minimum uncertainty limit of the critical repose angle considered in [44]. Case C is an ideal assumption of 1D debris bed. Three cases are assumed as homogenous debris bed with effective diameter of 2.5 mm, which is the middle value of the two homogenous cases in Table 4.1.

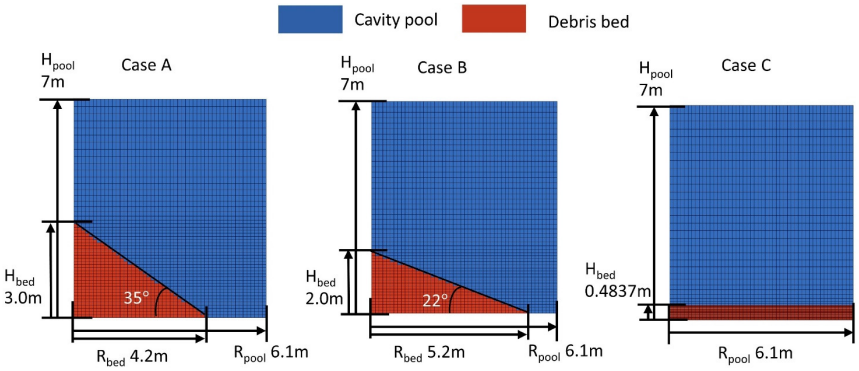

Figure 4.4 The computational domains for three cases with different bed slope angle.

The debris bed temperature evolution for three cases is shown in Figure 4.5~Figure 4.7. The arrows are the coolant velocity vectors, green solid ones for liquid phase and white dashed ones for gas phase. Case A and Case B have similar quench front propagation. The natural circulation is observed where the liquid coolant in the bed is heated to steam, and the steam flows up and exits the bed. The hot debris is quenched gradually with the coolant penetration from the surface near bottom. The quench front propagates from the bed bottom to the central top. Case C has one-dimensional quench front along the axial direction from the top of the bed to the bottom. The coolant velocity is generally in axial direction, and the downward liquid flow is hindered by the upward steam flow. The maximum temperature of the debris bed occurs at the place where the liquid coolant could penetrate last. For Case A and Case B, the maximum temperature occurs on the central top of the bed. For Case C, the maximum temperature occurs at the bottom.

The quenched mass fraction with time for three cases is plotted in Figure 4.8. The green dashed line for Case C seems to be linear, which means approximately constant quench rate, due to its one-dimensional quench front propagation. With the decrease of bed slope angle (from Case A to Case C), it takes less time to quench and correspondingly has lower temperature increase for local unquenched region. Figure 4.9 shows the debris bed mass fraction with a temperature increase higher than the x-axis value before quenched. Less than 3% mass has the temperature increase of 400 K for Case A, and 300 K for Case B. Since the self-leveling

could decrease the slope angle, the present simulation without the consideration of debris bed self-leveling should be conservative.

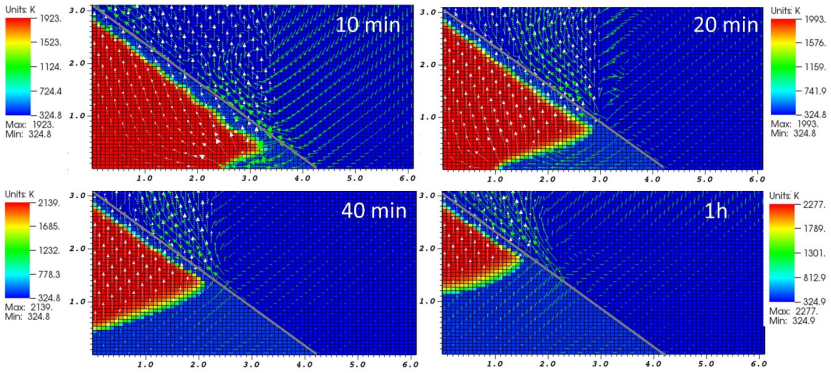

Figure 4.5 Temperature evolution for Case A.

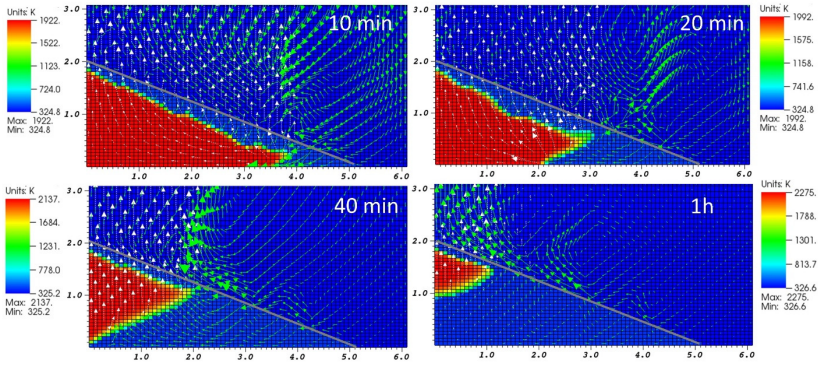

Figure 4.6 Temperature evolution for Case B.

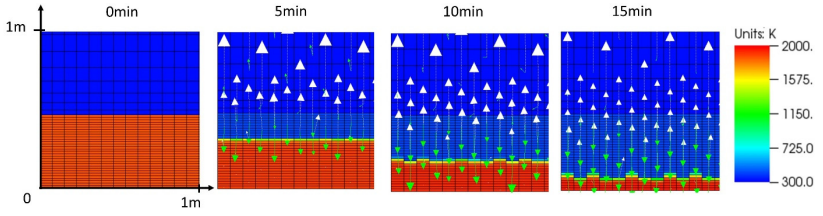

Figure 4.7 Temperature evolution for Case C.

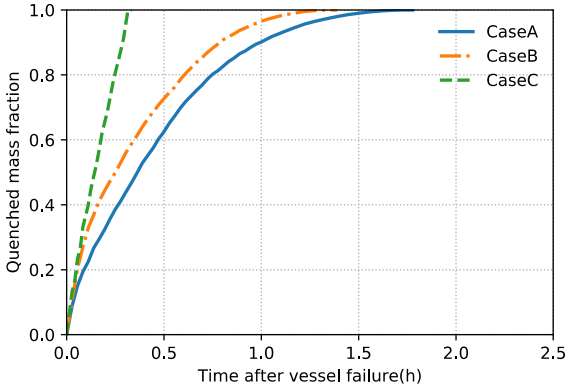

Figure 4.8 Mass fraction of quenched debris bed with time for Cases A, B and C.

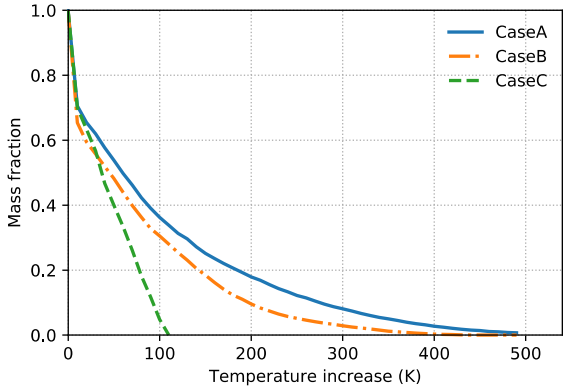

Figure 4.9 Mass fraction of the debris bed with the temperature increase for Cases A, B and C.

Figure 4.10 shows containment pressure including three coupled simulation cases and the MELCOR standalone case. After vessel failure, the initially highly subcooled cavity pool is heated by the released debris. The containment pressure increases fast after the pool saturated, until reaching the critical value of the containment venting. Then pressure drops due to the activation of containment venting.

Three coupled cases predict similar containment transient. MELCOR standalone simulation predicts a later time to reach the cavity pool

saturation and the containment venting. In MELCOR standalone simulation, the temperature of the one-layer corium in cavity remains above 1000 K at 10 h after vessel failure. While in coupled simulations, the debris beds are fully quenched to the pool temperature in less than 1.5 hours. The energy transferred from the debris bed to the pool is much faster in the coupled simulations than MELCOR standalone simulation. Therefore, a faster pressure transient is predicted in coupled simulations.

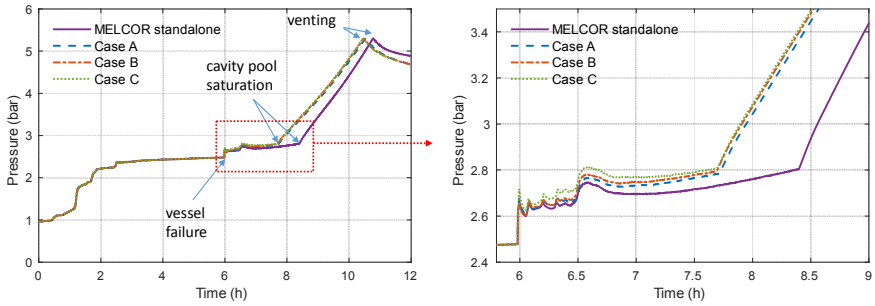

Figure 4.10 Containment pressure for MELCOR standalone and coupled cases.

4.2 Long-term coolability

The long-term behavior of a debris bed is a complex phenomenon. From the knowledge and experiences accumulated from the Chernobyl and Fukushima severe accidents, a debris bed could have e.g., possible clogging of by sediments, degradation and fracturing of debris particles after leaching, corrosion and self-irradiation, etc. [48]. All these possible aspects could affect the long-term coolability of debris bed, but the current knowledge of certain phenomena is still not sufficient to consider them in this work.

The long-term coolability discussed in the present study is estimated based on the comparison between decay power density and dryout power density of a debris bed. A debris bed is considered non-coolable as long as the decay power density is higher. Based on this assumption, the MELCOR and surrogate model coupled simulation is performed, where the dryout power density is predicted by the surrogate model and compared with the decay power for the quick estimation of the debris bed coolability.

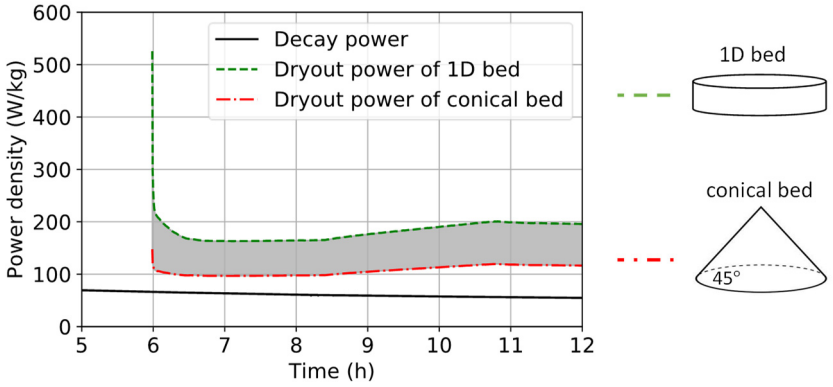

Figure 4.11 Power density of decay and dryout for two debris beds.

Figure 4.11 shows the dryout power density if a 1D debris bed (green dashed line) or a conical debris bed (red dash-dotted line) formed in the cavity pool, in comparison with the decay power density (black solid line). The debris beds assume effective particle diameter of 2.5 mm, and the porosity of 0.42. The decay power is lower than the dryout power density, which means the dryout condition is not reached according to the simulation. If the self-leveling phenomena promotes the debris bed spreading from a conical shape towards a flat shape, the safety margin would be increased.

4.2.1 Coolability maps

The mass-averaged decay power density at the vessel failure time for the Nordic BWR is considered as a criterion to evaluate the coolability of a debris bed. The surrogate model is employed to estimate the dryout of a debris bed with properties in a certain range. Based on the result, the coolability maps are generated, as shown in Figure 4.12. Each map plots the dryout power density with the variation of porosity (y-axis) and effective particle diameter (x-axis), at a certain slope angle.

The dryout power density is colored in red if it is less than the decay power density at vessel failure time, and colored in blue if it is larger. The red area roughly represents the non-coolable condition, which is located at small values of porosity and particle diameter. The red area increases with the increase of slope angle, meaning that there is more chance to have non-coolable debris bed if larger slope angle is observed.

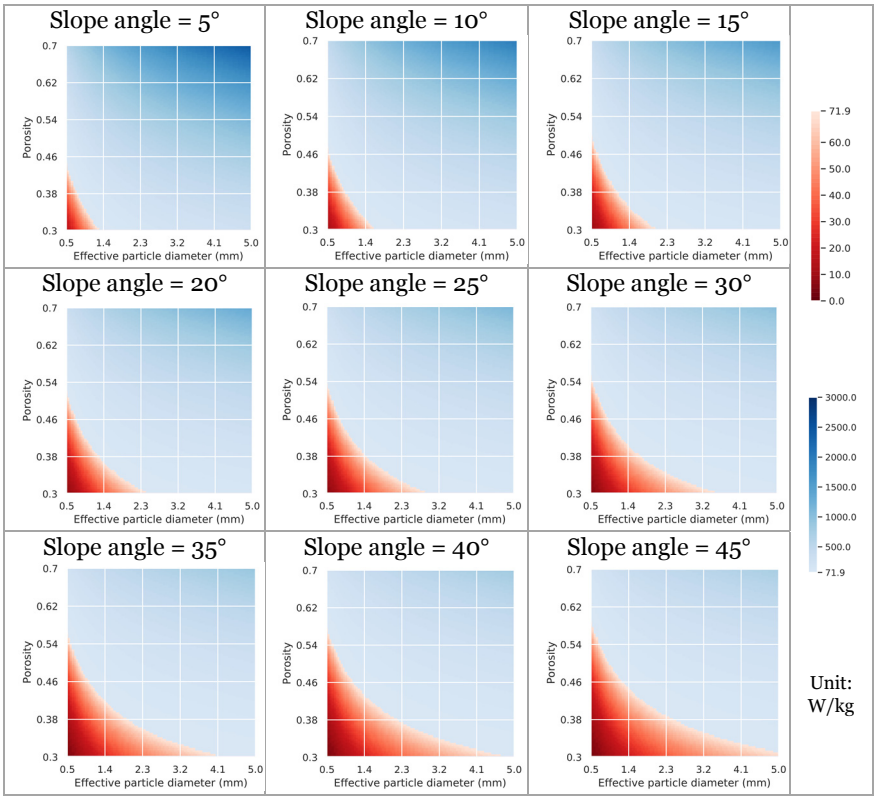

Figure 4.12 Dryout power density with the variation of porosity and effective particle diameter at different slope angle.

4.2.2 Sensitivity analysis

In order to evaluate the effect of the six input parameters in the surrogate model, the sensitivity analysis is performed with two methods: Spearman ranking and Sobol method. Spearman correlation is used to show the positive or negative linear relationship between parameter and the model output. The Sobol method is used to quantify the influence of the nonlinear relationships.

The Spearman correlation is defined as

$$\rho_s = \frac{\sum_N (X_N - \bar{X})\,(Y_N - \bar{Y})}{\sqrt{\sum_N (X_N - \bar{X})^2 \sum_N (Y_N - \bar{Y})^2}} \tag{4.1}$$

where X is the parameter; Y is the output; and N is the sample size.

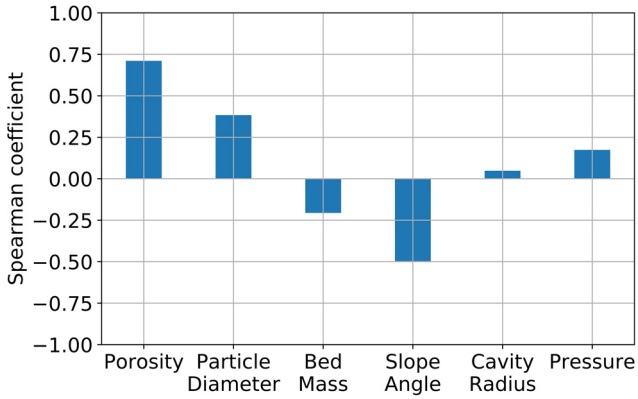

Figure 4.13 Spearman coefficients for parameters.

As a result, the Spearman coefficients between each input parameter and the dryout power density predicted from the surrogate model are shown in Figure 4.13. Positive relationships are observed for pressure, particle diameter, and porosity, meaning that higher values of these parameters would cause higher dryout power density, thus promote the debris bed coolability. On the contrary, slope angle and bed mass show negative relationship. Because higher values of slope angle and bed mass would require deeper penetration of the coolant, thus decrease the coolability.

The Sobol method is variance-based, and able to quantitatively measure the effect of one parameter singly or one combined with other parameters. It is computationally costly, and a common practice usually requires the model to run for 10^4 times [49]. It decomposes the variance of model output Y as the sum of the variance of each parameter and the variance of their interactive terms:

$$Var(Y) = \sum_{i}^{D} V_i + \sum_{i}^{D} \sum_{i<j} V_{ij} + \cdots + V_{1,2\ldots D} \tag{4.2}$$

where

$$V_i = Var\big(E(Y|X_i)\big) \tag{4.3}$$

$$V_{ij} = Var\left(E\left(Y|X_i, X_j\right)\right) - V_i - V_j \tag{4.4}$$

D is the input parameter dimension and E is the expectation operator. The first order effect is calculated as the fraction of the single parameter to the total variance of the model output as:

$$S_i = \frac{V_i}{Var(Y)} \tag{4.5}$$

Total effect represents the total contribution of one parameter to the variance of the model output, which is the sum of first order effect and higher order effect, calculated as:

$$S_{Ti} = S_i + \sum_{j}^{D} S_{ij} + \sum_{j}^{D}\sum_{k}^{D} S_{ijk} + \cdots \tag{4.6}$$

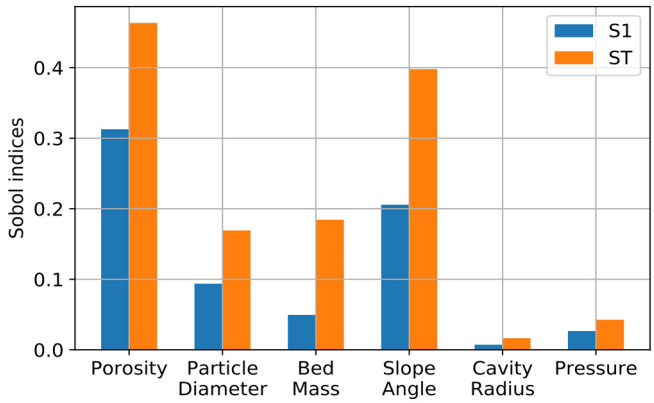

Figure 4.14 Sobol indices for parameters.

The Sobol indices for the six parameters are calculated and shown in Figure 4.14. It can be found that the porosity and the slope angle are most influential parameters decided by both first order and total effect. The large difference between first order and total indices indicates the existence of nonlinear terms in the model playing an important role. The attention should be paid to find the prototypical values due to the great impact of the bed properties.

4.2.3 Uncertainty analysis

The uncertainty analysis is performed for the ex-vessel debris bed coolability, under the framework shown in Figure 4.15. The uncertainty propagation through the models is achieved by sampling and massive simulation. The final goal is to estimate the non-coolable probability of the ex-vessel debris bed.

The model coefficients are considered as the MELCOR uncertainty sources, as listed in Table 4.3. The sampling is performed for each uncertain model coefficient based on its uncertainty distribution. MELCOR simulates with the sampled coefficients, and predicts the vessel failure time, the total bed mass, and the containment pressure.

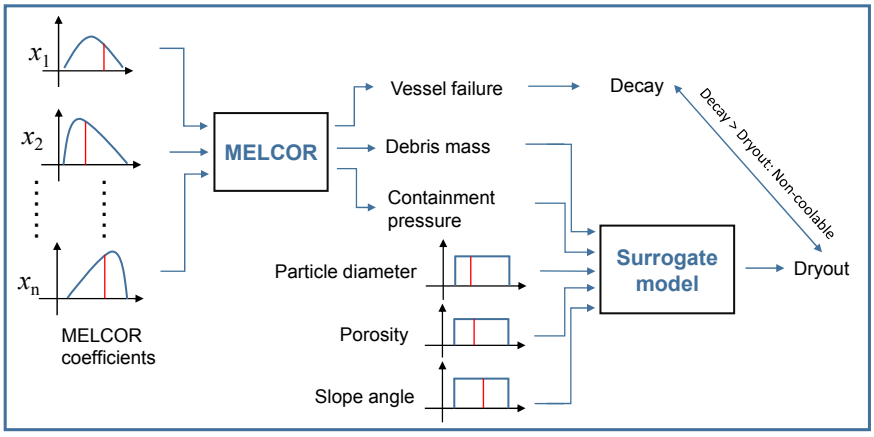

Figure 4.15 Uncertainty analysis framework.

For each case, the particle diameter, porosity, and slope angle are sampled from uniform distribution of their uncertain range, due to the scarce knowledge on their likely distribution. The surrogate model is run to estimate the dryout power density. The model error obtained in Chapter 3.2.1 is also considered as an uncertainty source, and used as a multiplier to the surrogate model output. The dryout power density is compared with the decay power density at vessel failure time. A non-coolable case is considered if decay power density is higher than dryout power density. The uncertain ranges of particle diameter, porosity, and slope angle are investigated by using different range options, as listed in Table 4.4.

Table 4.3 MELCOR model parameter uncertainties

No	Variables	Distribution	Range
1	time constants for radial (solid) debris relocation	Beta (1.33,1.67)	[180,720]
2	time constants for radial (liquid) debris relocation	Beta (1.33,1.67)	[30,120]
3	dT/dz model, time constant for averaging hydrodynamic material flows	Beta (1.1,1.1)	[0.09,0.11]
4	dT/dz model, characteristic time for coupling dT/dz temperatures to average CVH volume temperature when dT/dz model is active	Beta (1.1,1.1)	[8,12]
5	dT/dz model, maximum relative weight of old flow in smoothing algorithm involving time constant for averaging flows	Beta (1.1,1.1)	[0.5,0.7]
6	molten zircaloy melt break-through temperature	Beta (2.77,2.33)	[2100,2540]
7	molten cladding (pool) drainage rate	Beta (1.1111,1.8889)	[0.1,2.0]
8	fraction of strain at which lower head failure occurs	Beta (1.1,1.1)	[0.16,0.20]
9	minimum debris porosity (Lipinski dry-out model)	Beta (1.1,1.1)	[0.01,0.2]
10	minimum porosity to be used in calculating the flow resistance in the flow blockage model	Beta (1.1,1.1)	[0.01,0.2]
11	minimum porosity to be used in calculating the area for heat transfer to fluid	Beta (1.1,1.1)	[0.01,0.2]
12	porosity used in flow blockage Ergun pressure drop equation	Beta (1.1,1.1)	[0.01,0.2]
13	hydrodynamic volume fraction	Beta (1.1,1.1)	[0.01,0.2]
14	fraction of un-xidized cladding thickness at which thermal-mechanical weakening of oxidized cladding begins	Beta (1.1,1.1)	[0.0005,0.0015]
15	debris falling velocity	Beta (0.85,1.44)	[0.01,1.0]
16	debris quenching heat transfer coefficient to pool	Beta (1.1,1.1)	[100,2000]
17	candling heat transfer coefficients	Beta (1.1,1.1)	[1000,2000]

Table 4.4 Surrogate model input uncertain range options and CDF of non-coolable debris bed

Uncertain ranges	Particle size (mm)	Porosity	Slope angle (°)	Non-coolable probability
Option 1	(0.5, 5.0)	(0.3, 0.7)	(22, 35)	9.0%
Option 2	(1.5, 5.0)	(0.3, 0.7)	(22, 35)	5.0%
Option 3	(0.5, 5.0)	(0.4,0.7)	(22, 35)	4.2%
Option 4	(0.5, 5.0)	(0.3, 0.7)	(0, 22)	3.3%

For each case, a value called “power density difference” is calculated by the dryout power density minus the decay power density at the vessel failure time. If this value is positive, this case is considered as a coolable case, and vice versa. As a result, the empirical cumulative distribution function (CDF) for this power density difference in terms of the four uncertain range options is shown in Figure 4.16 (a). The negative domain of Figure 4.16 (a) is zoomed in and plotted as Figure 4.16 (b). It can be found that for the four uncertain range options, most sample cases are in the positive domain, which indicates the high probability to have coolable debris beds. There exist non-coolable cases, though in low probability, as represented by the negative domain. The non-coolable probability for each uncertain range option is listed in Table 4.4. It varies from 3.3% to 9.0%, which shows the strong impact of the uncertain input ranges.

It should be noted that the long-term coolability addressed here is only concerned with the removal of decay heat by natural circulation of saturated coolant. It is a conservative assumption because there is a chance that the debris bed is cooled by steam or radiation, and therefore a new stabilization of corium at a higher temperature below melting point may be established. Therefore, it is not a strictly non-coolable condition when the decay heat is higher than the dryout power to a certain extent. The initial condition of the debris bed is set as saturated, and therefore the quenching of the initially high-temperature debris beds is also not considered here.

The remaining factors can be considered as uncertain parameters in the future investigation to obtain a more comprehensive picture of debris bed coolability, including the avoidance of any excessive conservatism.

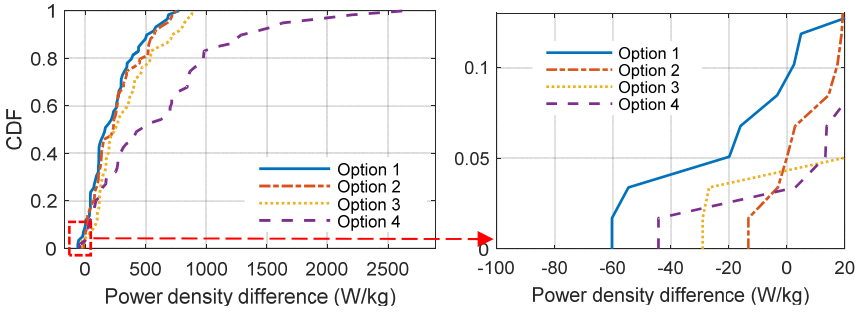

Figure 4.16 Cumulative distribution function (CDF) vs difference between dryout power density and decay power density at vessel failure time, for the four uncertainty range options in Table 4.4.

4.3 Summary

This chapter discusses the application of the developed tools to the safety analysis of Nordic BWRs.

The MELCOR/COCOMO coupled simulation is used to investigate the ex-vessel debris bed being quenched in the lower drywell pool under prototypical condition. The analysis suggests that the effective particle diameter employed for the prototypical debris bed should be approximately 10% larger than the Sauter mean diameter of the debris particles. The effect of debris bed shape shows that with a decrease in slope angle, the debris bed is quenched faster. Compared with MELCOR standalone simulation, coupled simulation predicts an earlier time to reach the pool saturation and containment venting.

The MELCOR and surrogate model coupled simulation is performed for Nordic BWR scenario as an illustration of its capability. The surrogate model alone is also applied to generate coolability maps, with which the debris bed coolability can be quickly observed given certain bed properties. The sensitivity analysis is performed to quantify the effect of the input parameters, which shows the porosity and slope angle are the most influential. The uncertainty analysis provides preliminary result on the debris bed non-coolable probability under certain accident scenario, but also shows that the probability could be affected by the uncertainty range of the bed properties.

5 Conclusions and outlook

5.1 Conclusions

The capability of severe accident system code MELCOR is developed in this thesis, for analyses of ex-vessel debris bed coolability in a deep water pool used for quenching and long term cooling as a part of SAM strategy at Swedish NPPs. For that, MELCOR is coupled with two external codes: (i) the COCOMO code; and (ii) a surrogate model. The coupled MELCOR/COCOMO simulation can predict the quench process, and the coupled MELCOR/surrogate model can predict the cooling limit of debris bed with high computational efficiency.

To set up the proper MELCOR model for a reference Nordic BWR, a nodal sensitivity study of MELCOR simulation is first conducted for postulated severe accident scenarios of the BWR plant, using three core meshes. It is found that the coarse mesh (6 rings of the core) predicts an earlier vessel failure and a faster corium release, which makes a more conservative precondition for the analysis of debris bed coolability. As a result, the 6-ring core mesh is selected for the coupled simulation.

In the coupled MELCOR/COCOMO simulation, the MELCOR code is used for integral simulation of accident progression, while the COCOMO code is employed specifically to calculate the heat transfer between debris particles and the two-phase flow at natural convection in the cavity pool. MELCOR provides COCOMO the initial and boundary conditions for the water pool in the reactor cavity and some properties for the debris bed including its initial temperature, total mass, and decay power. COCOMO characterizes the heat transfer rate from debris bed to the water pool, for MELCOR to simulate the response of the plant. Data exchange is achieved via the coupling interface, where an asynchronous coupling approach is used.

Due to the limitations of COCOMO for fast calculations, a surrogate model is developed to estimate the dryout power density of a two-dimensional debris bed. The dryout power density is the maximum power density

removed in a debris bed under steady state, treated as a cooling limit of long-term coolability. A characteristic factor, proposed to represent the influence of two-dimensional features of a debris bed, is used as a multiplier to the prediction of Lipinski model. With the Kriging method, the characteristic factor is correlated to six parameters of the debris bed influencing coolability: debris bed open porosity, particle diameter, debris bed mass, slope angle, base radius, and ambient pressure. The obtained surrogate model predicts the dryout power density in a satisfactory agreement with COCOMO (full model), within the maximum deviation of $\pm 10\%$ relative.

The developed simulation tools are applied in the safety analysis for the Nordic BWR with adopted SAM strategy. The coupled MELCOR/COCOMO simulation is used to investigate the quenching process of an ex-vessel debris bed formed in the lower drywell under a prototypical condition. Assuming the particle size distribution of a conical debris bed is the same as that measured in FARO L31 test, the effective particle diameter is found to be approximately 10% larger than the Sauter mean diameter of all the debris particles, quantified by the mass-averaged quench rate and maximum temperature increase.

The effect of debris bed shape is also investigated, and the results indicate that the quench front propagation is driven by flow patterns inside the debris beds. The decrease in slope angle is found favorable for faster quenching of the debris bed particles. The 1D debris bed with zero slope angle reaches the maximum quench rate. Compared with a MELCOR standalone analysis, the coupled MELCOR/COCOMO simulation predicts an earlier saturation of the water pool in the lower drywell and an earlier activation of containment venting system.

The coupled MELCOR and surrogate model simulation is performed for the Nordic BWR with a postulated severe accident. The results show that ex-vessel debris beds are coolable under prototypical conditions with probable bed properties. The surrogate model alone is also used to generate coolability maps, helping to assess coolability of debris bed as long as the properties of the debris bed are predicted and they are within the variation ranges of the model. A sensitivity analysis shows the porosity and the slope angle of a debris bed are the most influential parameters for debris bed coolability. An uncertainty analysis methodology is proposed to obtain the probability of non-coolable debris beds, and the results also

show that the uncertainties in characterization of debris beds are important.

5.2 Outlook

In the coupled MELCOR/COCOMO simulation conducted in the present study, assumptions and simplifications are made, which may affect the results and can be addressed in future studies. For instance, the oxidation of the metallic materials in debris is not considered, of which the reaction heat and hydrogen generation would possibly hinder the coolability and containment response. The re-melting of the debris bed should be concerned if it is not coolable. The ability to better simulate the debris bed formation process would definitely help to capture more realistic accident scenario.

More accurate quantification of debris bed properties (e.g., porosity and shape) should be focused, since they are found to be very influential on the coolability, but we still have a lack of reliable data for prototypical conditions. The uncertainty range and distribution of the debris bed properties are also desired.

The surrogate model developed in this work for determination of dryout power could be further extended to predict characteristic features during quench process.

Instead of code coupling, additional benefits for more details of complex reactor system behavior during the ex-vessel phase of a severe accident can be received after direct implementation of particulate debris bed coolability model in MELCOR code.

Bibliography

[1] "Strålsäkerhetsmyndigheten (SSM) - Swedish National Action Plan Response to ENSREG's request within the European Stress Tests," revision 1, December, 2014.

[2] S. A. Hodge, "BWR reactor vessel bottom head failure modes," Boiling Water Reactor Severe Accident Technology (BWRSAT) Program, Oak Ridge National Laboratory, 1989.

[3] D. Magallon and I. Huhtiniemi, "Corium melt quenching tests at low pressure and subcooled water in FARO," vol. 204, pp. 369–376, 2001.

[4] I. Lindholm, "A Review of Dryout Heat Fluxes and Coolability of Particle Beds," SKI report 02:17, 2002.

[5] L. Manickam, G. Qiang, W. Ma, and S. Bechta, "An experimental study on the intense heat transfer and phase change during melt and water interactions," *Exp. Heat Transf.*, vol. 32, no. 3, pp. 251–266, 2019.

[6] N. Chikhi and F. Fichot, "Experimental and theoretical study of large scale debris bed reflood in the PEARL facility," *Nucl. Eng. Des.*, vol. 312, pp. 48–58, Feb. 2017.

[7] N. K. Tutu, T. Ginsberg, J. Klein, J. Klages, and C. E. Schwarz, "Debris bed quenching under bottom flood conditions (in-vessel degraded core cooling phenomenology)," NUREG/CR--3850, United States, 1984.

[8] P. Schäfer, M. Groll, and R. Kulenovic, "Basic investigations on debris cooling," *Nucl. Eng. Des.*, vol. 236, no. 19–21, pp. 2104–2116, Oct. 2006.

[9] V. X. Tung and V. K. Dhir, "Quenching of debris beds having variable permeability in the axial and radial directions," *Nucl. Eng. Des.*, vol. 99, no. C, pp. 275–284, Feb. 1987.

[10] D. H. Cho, D. R. Armstrong, and S. H. Chan, "On the pattern of penetration into a hot particle bed," *Nucl. Technol.*, vol. 65, no. 1,

pp. 23–31, 1984.

[11] Z. Huang and W. Ma, "Validation and application of the MEWA code to analysis of debris bed coolability," *Nucl. Eng. Des.*, vol. 327, pp. 22–37, 2018.

[12] K. Hu and T. G. Theofanous, "On the measurement and mechanism of dryout in volumetrically heated coarse particle beds," *Int. J. Multiph. Flow*, vol. 17, no. 4, pp. 519–532, 1991.

[13] J. D. Gabor, J. C. Hesson, L. Baker Jr, and J. C. Cassulo, "Simulation experiments on hear transfer from fast reactor fuel debris," *Trans. Amer. Nucl. Soc.*, vol. 15, no. 2, p. 836, 1972.

[14] K. Atkhen and G. Berthoud, "SILFIDE experiment: Coolability in a volumetrically heated debris bed," vol. 236, pp. 2126–2134, 2006.

[15] H. C. Hardee and R. H. Nilson, "Natural convection in porous media with heat generation," *Nucl. Sci. Eng.*, vol. 63, no. 2, pp. 119–132, 1977.

[16] E. S. Sowa, J. C. Hesson, R. H. Gebner, and G. T. Goldfuss, "Heat transfer experiments through beds of UO2 in boiling sodium," *Trans. Amer. Nucl. Soc.*, vol. 14, no. 2, p. 725, 1971.

[17] R. J. Lipinski, "A model for boiling and dryout in particle beds," Sandia National Laboratories Report. NUREG/CR-2646, SAND82-0765, 1982.

[18] V. E. Schrock, C. H. Wang, S. Revankar, L. H. Wei, S. Y. Lee, and D. Squarer, "Flooding in particle beds and its role in dryout heat flux prediction." 1986.

[19] A. Karbojian, W. M. Ma, P. Kudinov, and T. N. Dinh, "A scoping study of debris bed formation in the DEFOR test facility," vol. 239, pp. 1653–1659, 2009.

[20] M. Bürger, M. Buck, W. Schmidt, and W. Widmann, "Validation and application of the WABE code: Investigations of constitutive laws and 2D effects on debris coolability," *Nucl. Eng. Des.*, vol. 236, no. 19–21, pp. 2164–2188, Oct. 2006.

[21] E. Takasuo, S. Holmström, T. Kinnunen, and P. H. Pankakoski, "The COOLOCE experiments investigating the dryout power in debris beds of heap-like and cylindrical geometries," *Nucl. Eng. Des.*, vol. 250, pp. 687–700, 2012.

[22] Z. Huang and W. Ma, "Numerical investigation on quench of an ex-

vessel debris bed at prototypical scale," *Ann. Nucl. Energy*, vol. 122, pp. 47–61, 2018.

[23] T. Szabó, F. Kretzschmar, and T. Schulenberg, "Obtaining a more realistic hydrogen distribution in the containment by coupling MELCOR with GASFLOW," *Nucl. Eng. Des.*, vol. 269, pp. 330–339, 2014.

[24] Z. Huang and W. Ma, "Performance of a passive cooling system for spent fuel pool using two-phase thermosiphon evaluated by RELAP5/MELCOR coupling analysis," *Ann. Nucl. Energy*, vol. 128, pp. 330–340, 2019.

[25] P. Dietrich, "Expansion of the Severe Accident Code MELCOR by Coupling External Models," KIT Scientific Publishing, Karlsruhe, 2016.

[26] A. Bonelli *et al.*, "Station black-out analysis with MELCOR 1.8.6 code for atucha 2 nuclear power plant," *Sci. Technol. Nucl. Install.*, vol. 2012, 2012.

[27] L. L. Humphries, B. A. Beeny, F. Gelbard, D. L. Louie, and J. Phillips, "MELCOR Computer Code Manuals Vol.1: Primer and Users' Guide," Albuquerque, NM 87185-0748, 2017.

[28] L. Nilsson, "Development of an Input Model to MELCOR 1.8.5 for Oskarshamn 3 BWR," SKI Report 2007:05, 2007.

[29] B. Pershagen, *Light Water Reactor Safety*. 1989.

[30] F. R. Larson and J. Miller, "A Time-Temperature Relationship for Rupture and Creep Stress," *Trans. ASME*, pp. 765–775, 1952.

[31] S. Ergun, "Fluid Flow through Packed Columns," *Chem. Eng. Prog*, vol. 48, no. 2, pp. 89–94, 1952.

[32] G. Hofmann and T. Schulenberg, "A quasi-steady-state approximation to the transient dryout behavior in debris beds," in *Proc. of the international meeting on light water severe accident evaluation*, 1983.

[33] R. J. Lipinski, "A Model for Boiling and Dryout in Particle Beds," Sandia National Laboratories,NUREG/CR-2646 SAND82-0765, 1982.

[34] A. W. Reed, "The effect of channeling on the dryout of heated particulate beds immersed in a liquid pool (Ph.D Thesis)," Massachusetts Institute of Technology, Cambridge, USA., 1982.

[35] T. Schulenberg and U. Müller, "A refined model for the coolability of core debris with flow entry from the bottom," in *Proceedings of the Sixth Information Exchange Meeting on Debris Coolability*, 1986.

[36] V. X. Tung and V. K. Dhir, "A hydrodynamic model for two-phase flow through porous media," *Int. J. Multiph. Flow*, vol. 14, no. 1, pp. 47–65, Jan. 1988.

[37] W. Schmidt, "Influence of multidimensionality and interfacial friction on the coolability of fragmented corium (Ph.D thesis)," Universität Stuttgart, Germany, 2004.

[38] Z. Huang, "Numerical Investigations on Debris Bed Coolability and Mitigation Measures in Nordic Boiling Water Reactors (Ph.D thesis)," KTH Royal Institute of Technology, Sweden, 2019.

[39] L. Li, W. Ma, and S. Thakre, "An experimental study on pressure drop and dryout heat flux of two-phase flow in packed beds of multi-sized and irregular particles," *Nucl. Eng. Des.*, vol. 242, pp. 369–378, 2012.

[40] E. Takasuo, "A summary of studies on debris bed coolability and multi-dimensional flooding," NKS-374 ISBN 978-87-7893-459-8, VTT Technical Research Centre of Finland Ltd, 2016.

[41] B. W. Spencer, K. Wang, C. A. Blomquist, L. M. McUmber, and J. P. Schneider, "Fragmentation and quench behavior of corium melt streams in water," NUREG/CR-6133, ANL-93/32, Nuclear Regulatory Commission, Washington, DC, USA, 1994.

[42] P. Kudinov, A. Karbojian, C. T. Tran, and W. Villanueva, "Agglomeration and size distribution of debris in DEFOR-A experiments with Bi2O3-WO3 corium simulant melt," *Nucl. Eng. Des.*, vol. 263, pp. 284–295, 2013.

[43] N. Chikhi *et al.*, "Evaluation of an effective diameter to study quenching and dry-out of complex debris bed," *Ann. Nucl. Energy*, vol. 74, pp. 24–41, 2014.

[44] S. Basso, A. Konovalenko, S. E. Yakush, and P. Kudinov, "The effect of self-leveling on debris bed coolability under severe accident conditions," *Nucl. Eng. Des.*, vol. 305, pp. 246–259, Aug. 2016.

[45] M. A. Bouhlel, J. T. Hwang, N. Bartoli, R. Lafage, J. Morlier, and J. R. R. A. Martins, "A Python surrogate modeling framework with derivatives," *Adv. Eng. Softw.*, p. 102662, Jul. 2019.

[46] W. Ma and T. Dinh, “The effects of debris bed ’ s prototypical characteristics on corium coolability in a LWR severe accident,” vol. 240, pp. 598–608, 2010.

[47] W. Hilali, “Debris Bed Formation in Degraded Cores of Light Water Reactors,” Universität Stuttgart, 2019.

[48] OECD/NEA, “Long-Term Management and Actions for a Severe Accident in a Nuclear Power Plant,” No.7506, 2021.

[49] B. Iooss and P. Lemaître, “A review on global sensitivity analysis methods,” *Oper. Res. Comput. Sci. Interfaces Ser.*, vol. 59, pp. 101–122, 2015.